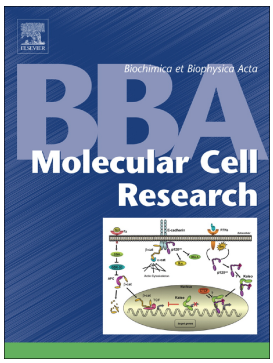

Molecular insight on the altered membrane trafficking of TrkA kinase dead mutants

Rosy Amodeo, Riccardo Nifosì, Chiara Giacomelli, Cosetta Ravelli, Letizia La Rosa, Andrea Callegari, Maria Letizia Trincavelli, Stefania Mitola, Stefano Luin, Laura Marchetti

PII: S0167-4889(19)30222-8

DOI: https://doi.org/10.1016/j.bbamcr.2019.118614

Reference: BBAMCR 118614

To appear in: *BBA - Molecular Cell Research*

Received date: 15 April 2019

Revised date: 11 November 2019

Accepted date: 18 November 2019

Please cite this article as: R. Amodeo, R. Nifosì, C. Giacomelli, et al., Molecular insight on the altered membrane trafficking of TrkA kinase dead mutants, *BBA - Molecular Cell Research*(2019), https://doi.org/10.1016/j.bbamcr.2019.118614

Molecular insight on the altered membrane trafficking of TrkA kinase dead mutants

Rosy Amodeo[1,2,*], Riccardo Nifosì[3,1], Chiara Giacomelli[4], Cosetta Ravelli[5], Letizia La Rosa[6], Andrea Callegari[1,#], Maria Letizia Trincavelli[4], Stefania Mitola[5], Stefano Luin[1,3], Laura Marchetti[2,4*]

[1] NEST, Scuola Normale Superiore, Pisa, Italy

[2] Center for Nanotechnology Innovation @NEST, Istituto Italiano di Tecnologia, Pisa, Italy

[3] NEST, Istituto Nanoscienze-CNR, Pisa, Italy

[4] Department of Pharmacy, University of Pisa, Pisa, Italy

[5] Department of Molecular and Translational Medicine, University of Brescia, Brescia, Italy

[6] Bio@SNS, Scuola Normale Superiore, Pisa, Italy

[#] current address: Cell Biology and Biophysics Unit, European Molecular Biology Laboratory (EMBL), Heidelberg, Germany

* corresponding authors: rosy.amodeo@sns.it, laura.marchetti@unipi.it

Abstract

We address the contribution of kinase domain structure and catalytic activity to membrane trafficking of TrkA receptor tyrosine kinase. We conduct a systematic comparison between TrkA-wt, an ATP-binding defective mutant (TrkA-K544N) and other mutants displaying separate functional impairments of phosphorylation, ubiquitination, or recruitment of intracellular partners. We find that only K544N mutation endows TrkA with restricted membrane mobility and a substantial increase of cell surface pool already in the absence of ligand stimulation. This mutation is predicted to drive a structural destabilization of the αC helix in the N-lobe by molecular dynamics simulations, and enhances interactions with elements of the actin cytoskeleton. On the other hand, a different TrkA membrane immobilization is selectively observed after NGF stimulation, requires both phosphorylation and ubiquitination to occur, and is most probably related to the signaling abilities displayed by the wt but not mutated receptors. In conclusion, our results allow to distinguish two different TrkA membrane immobilization modes and demonstrate that not all kinase-inactive mutants display identical membrane trafficking.

Keywords

TrkA receptor, VEGFR2 receptor, tyrosine kinase domain, membrane dynamics, molecular dynamics, mutation.

1. Introduction

Receptor tyrosine kinases (RTKs) constitute a large superfamily of 58 known membrane receptors; these are activated by a wide array of growth factors, and mediate fundamental biological functions including cell growth and survival, cell-to-cell communication, differentiation, and metabolism [1], [2]. RTKs share an extracellular domain that interacts with the ligand, a single transmembrane α-helix and an intracellular domain that contains the catalytic tyrosine kinase domain (TKD). The TKD consists of two lobes, with antiparallel β-sheets and one single α-helix (denoted as αC helix) in the N lobe, and a mainly α-helical C lobe. RTKs activation is regulated by a specific orientation of the activation loop connecting the N to the C lobe, required for both catalysis and phosphotransfer reactions [3]. A number of auto-inhibitory mechanisms exist, based e.g. on the position of αC helix, or on the conformation of the activation loop, which prevent TKD activation in the unbound state [1]. These are released upon ligand binding, which results in efficient activation of the kinase activity. The catalyzed phosphotransfer reaction from ATP onto the hydroxyl group of Tyr represents an important posttranslational modification (PTM), evolutionarily conserved from prokaryotes to humans. Accordingly, the TKD of RTKs is highly conserved.

A growing number of mutations in RTKs are being identified, which crucially contribute to cancer, type 2 diabetes, cardiovascular, neurodegenerative and developmental disorders [4]–[7]. Most of these occur in the TKD key regulatory elements. Typically, kinase hyperactivating mutations are found in cancer, and kinase inactivating mutations in developmental and other genetic disorders [8], [9]. Furthermore, mutations of the residues coordinating ATP or performing catalytic activity are found in a subfamily of RTKs named pseudokinases [2], [10]. Although lacking kinase activity, these proteins do have signaling abilities and play important

physiological and pathological roles. However, the molecular basis underlying the functions of kinase-inactivating or pseudokinase mutations has been poorly investigated.

Here, we study the impact of specific mutations in the TKD of the Nerve Growth Factor (NGF) receptor TrkA on its membrane dynamics, intracellular trafficking and PTMs. TrkA plays fundamental roles in development of the nervous system [11], [12], and is also an important player in carcinogenesis [13]. Mutations of TrkA sequence are reported both in cancer [13] and in HSAN IV genetic disease [14]. In particular, we focus our attention on the mutation of lysine 544 (human numbering) in the β3 sheet of the TKD N lobe, which is crucial to allocate ATP and thus to kinase activity; noteworthy, this mutation resembles those displayed by pseudokinases [2]. ATP binding to Lys 544 is an upstream event during TrkA TKD activation [15], [16]. This drives phosphorylation of Tyr of the activation loop (Y676, Y680, Y681 [17], [18]), and of scaffolding Tyr (Y496, Y757, Y791 [19]–[21]). Furthermore, Lys 544 was reported to be important for TrkA ubiquitination [22], [23]. We provide evidence that mutation of this Lys to Asn slows down membrane dynamics in a manner that paradoxically resembles that of NGF-activated TrkA-wt [24]. However, the two membrane immobilization modes have distinct structural and functional determinants, which are here characterized. Our observations may possibly be extended to other RTKs, thus providing interesting cues to the study of their genetic or somatic mutations.

2. Materials and methods

2.1 Note on sequences

We performed our studies both on the rat and human TrkA sequences. The two sequences share a very high homology (86% in the entire protein sequence, 94.6 % in the TKD).

Throughout the text, we shall use *h*TrkA and *r*TrkA to specify the human and rat sequences, respectively. Analogously, for Vascular Endothelial Growth Factor receptor 2 (VEGFR2), we used both the mouse and human sequences, which are renamed *m*VEGFR2 and *h*VEGFR2, respectively. The correspondence between numbering of residues in the different sequences is listed in Table S1 for TrkA and S2 for VEGFR2.

2.2 Constructs

ACP-tagged *r*TrkA construct was previously described [25]. S6-tagged *h*TrkA construct was previously described [26]. These constructs were used to generate all TrkA mutants, using the QuikChange mutagenesis kit (Agilent) and a pair of specific oligonucleotides (Sigma) for each desired mutation. Multiple mutations in KM and RM were introduced sequentially in the template sequence. cDNAs of *h*TrkA-wt, *h*TrkA-K544N and *h*TrkA-K544R were also cloned in an "all-in-one" third generation Tet-on lentiviral pTRE vector [27]. S6-*m*VEGFR2 construct was obtained inserting the S6 tag after the signal peptide of *m*VEGFR2 cDNA by GeneArt Synthesis (Thermo Scientific) and cloning it into pTRE lentiviral vector. *m*VEGFR2-K866N and *m*VEGFR2-K866R were prepared starting from the wt sequence using the QuikChange Site-Directed mutagenesis kit (Agilent) and a pair of specific oligonucleotides (Sigma) for each desired mutation. All mutations and relative primer sequences are reported in Table S3.

2.3 Single molecule labeling of surface TrkA and VEGFR2 constructs

After 5 hours from transfection, SHSY5Y or GM7373 cells were trypsinized and transferred into glass-bottom chambers (at a density of 2-3*10^5 cells per 22-mm-diameter WillCo® dish). Next day, cells were serum starved for 2 hours. Then surface receptors were labeled with Qdot as described previously [24], [27]. Briefly, cells were first biotinylated with a 30-minute

incubation at 37°C with 0.5% BSA, 1 µM Sfp synthase, 10 mM $MgCl_2$ and 2 µM of coA-biotin in starvation medium. After two washes in PBS, cells were incubated for 2 minutes at room temperature (RT) with 2 nM Qdot® 655 streptavidin conjugate (Invitrogen) in borate buffer pH 8.3, 0.5% BSA and 215 mM sucrose. Cells were washed eight times with PBS and left in medium. For TrkA, cells were then both unstimulated and stimulated with 125 ng/mL NGF diluted in starvation medium. Ligand addition was performed directly on the dish at the microscope, by adding a 250 ng/mL NGF solution in starvation medium to an equal volume of medium in the dish. Unless otherwise stated, cells were always imaged for a maximum of 15 minutes upon ligand addition.

2.4 Total internal reflection fluorescence (TIRF) microscopy

Labelled cells were imaged at 37°C, 5% CO_2 with a Leica DM6000 microscope equipped with a TIRF-AM module, incubator chamber, electron multiplying charge-coupled-device (CCD) camera (ImagEM C9100-13, Hamamatsu), and 100× oil immersion objective (NA 1.47). For live cell imaging, time series were acquired on a region of interest (ROI) with constant size of 32.7×34.5 µm within the basal membrane of each cell; Qdot655 was imaged using the 488 nm laser line, FF01-655/15 Semrock emission filter and a penetration depth of 110 nm. For single step photobleaching assay, we used a ROI of 32.68 x 32.68 µm and Abberior635 was excited using the 635 nm laser line with a penetration depth of 90 nm. The integration time per frame, corresponding to the lag time between two consecutive frames, was set at 21 ms and typical time series lasted 3000 frames.

2.5 Single-molecule internalization assay

Transfected or transduced SHSY5Y cells seeded in glass-bottom WillCo dishes were starved for 2 hours, receptors labelled with Qdot and transferred at the TIRF microscope. The automatized stage was used for saving the position of 4-5 fields in which a sizeable number of cells displayed Qdot moving particles. Then we added 125 ng/ml NGF to the medium and followed the cells in the selected fields in a time course of eight points (0, 5, 10, 15, 30, 40, 50 and 60 min); as control, we repeated a similar experiment without adding NGF. For each cell and time point, we quantified the membrane density as the number of labelled receptors within cell area (quantified from the relative DIC image), in order to measure enrichment or depletion of surface *r*TrkA-wt and -K547N receptors in the presence or absence of NGF stimulation. For comparing the internalization time-course of different cells, we normalized the spot density of each cell to its value at time 0. Cells with a similar (average) transgene expression levels were chosen, excluding those with a number of moving labelled receptors below 3.

2.6 Single step photobleaching assay

24 hours after doxycycline induction, SHSY5Y cells expressing *h*TrkA -wt, -K544N, -K544R were starved for 2 hours. Then all constructs were labelled for 30 minutes at 37°C with 20 nM CoA-Abberior635P, 1 µM Sfp synthase, 10 mM $MgCl_2$ in starvation medium. Cells were washed twice in PBS, fixed for 90 min at room temperature with 4% PFA/2% Sucrose/0.1% Glutaraldehyde in PBS (GA, Electron Microscopy Sciences), washed five times with PBS and imaged in PBS. Time series were then analyzed following the procedure reported in [28]: briefly, the background fluorescence was subtracted using the ImageJ software and then single spots were identified and detected as isolated fluorescent signals falling within a 3 x 3 pixels roi, so that the number of photobleach steps therein could be quantified.

2.7 Drug treatments

Cells were seeded in glass-bottom dishes, after 24 hours starved for 2 hours before or during the drug treatment, and finally fixed for 10 minutes at RT with 4% PFA. Cells were then washed twice with PBS, permeabilized for 4 minutes at RT with 0.1 % TritonX-100 in PBS (Sigma Aldrich), washed twice again and then blocked for 20 minutes at RT with 1% Bovine Serum Albumin (Sigma Aldrich) in PBS. After blocking, cells were incubated with Alexa Fluor 647-Phalloidin (Invitrogen) diluted 1:40 in blocking solution. Finally, cells were washed twice with PBS, once with water (Millipore), dried and mounted in Fluoroshield mounting medium (Sigma Aldrich). Samples were evaluated at the TIRF microscope, with penetration depth of 150 nm, using HCX PL APO 100X (NA 1.47) objective and a ROI of 58,4μm x58.4μm; excitation used the 488 nm laser line and emission was collected with a FF01-525/45-25 Semrock filter. Based on phalloidin staining, we defined as optimal the following incubations: i) 2h at 37°C with 1μM cytochalasin D (Sigma-Aldrich) during serum starvation before labelling; ii) 15 min at 37°C with 1 μM latrunculin B (Sigma-Aldrich) in the last half of labelling; iii) 30 min at 37°C with 100 nM jasplakinolide (Sigma-Aldrich) during labelling. Cells were then labelled as described previously, washed eight times with PBS, and then imaged in medium devoid of drugs.

2.8 Structural MD simulations

We performed Molecular Dynamics (MD) simulations of the *h*TrkA-wt TDK and of its K544N, K544R, K544P and K544A mutants, and of *h*VEGFR2 TKD and its K868N and K868R

mutants. The structure of *h*TrkA TKD was taken from the X-ray structure with PDB code 4f0i (starting with Cys501 and ending with Val790; [29] and that of VEGFR2 from PDB code 6gqq (Leu814 to Asn1168; [30]). For TrkA, two protein chains are present in the PDB file and we chose chain B as the starting structure because residues 535 and 536 are missing in chain A. The Reduce software [31] was used together with Whatif [32] to fix the orientation of Asn/Gln/His amino acids and detect the protonation of histidine residues. The two software packages gave the same results concerning the histidine buried inside the protein while they differed for some solvent exposed histidine. We considered an ε protonation for His 569, 594, 645, 648 and 772 in TrkA, and 816, 876, 879, 891, 895, 1004, 1026 and 1144 in VEGFR2, and δ protonation for all the other His residues. Mutations of Lys 544 (Lys868 in VEGFR2) to Asn, Arg, Pro and Ala were performed using the Rosetta software [33]. All proteins were solvated in a ~9 nm truncated octahedron box of ~17000 water molecules with a 0.1 M concentration of NaCl. The Amber ff99SB*-ILDN [34], [35] was used with TIP3P force field parameters for water. Within a periodic boundary condition set up, the system was subjected to geometry optimization by minimizing its total potential energy and then equilibrated with short MD simulations at constant temperature and pressure, applying restraints of decreasing strength to keep the non-hydrogen atoms of the protein close to the starting structure (20ps with 5000 kcal/mol $Å^{-2}$, 50ps with 3000 kcal/mol $Å^{-2}$ and 200ps with 1000 kcal/mol $Å^{-2}$). The equilibrated structures were used as starting points for 800ns-long production runs (600ns for VEGFR2). In the case of *h*TrkA-wt, -K544N and -K544R three different MD runs starting from the same geometry but different randomly assigned velocities were performed. Production runs employed a 2 fs time step (LINCS was used to constraint bonds involving H atoms), v-rescale thermostat (with a coupling of $\tau_T = 0.2$ ps) and Parrinello-Rahman barostat ($\tau_P = 5$ ps) to maintain a constant 300 K temperature and 1 bar pressure respectively. Snapshots were

saved each 10 ps and the first 100 ns of each MD trajectory were discarded in the analysis. Simulations and analyses were performed with the Gromacs 5 package [36].

2.9 Statistical analysis

Statistical analysis was performed with OriginPro v8.50 and GraphPad Prism 6 softwares, or with algorithms implemented in MatLAB. For most of experiments, we used a one-way ANOVA, with Bonferroni's means comparison. The time course of *r*TrkA-wt versus *r*TrkA-K547N internalization was analyzed with a two-way ANOVA. Non-parametric tests for analysis of two samples were performed with Mann–Whitney test, of more than two samples with Kruskal-Wallis test followed by Dunn's means comparison. Significance was set at α=0.05. For testing differences in D and L distributions we evaluated the error in each bin j considering the different weight w_{ji} in it for each trajectory i: the frequency f_j and its variance $\sigma_{f_j}^2$ was calculated as $f_j = \sum_{i=1}^{n} w_{ji}$, $\sigma_{f_j}^2 = \frac{n}{n-1}\left(\sum_{i=1}^{n} w_{ji}^2 - \frac{\left(\sum_{i=1}^{n} w_{ji}\right)^2}{n}\right)$ as in [37], where n is the total number of trajectories. Normalized frequencies and their error bars where calculated dividing f_j and σ_{f_j} by $\Delta \sum_j f_j$, where Δ is the bin width and the sum is over all bins. Differences in frequency counts in single-step photobleaching assay and in L distributions were analyzed using χ^2 tests, in D distributions were analyzed as described [28]. Each experiment was independently repeated at least twice, as indicated in detail in each figure caption along with the p values obtained.

3. Results

3.1 Membrane accumulation and immobilization of TrkA-K547N mutant

We previously performed single particle tracking (SPT) measurements of *r*TrkA and *h*TrkA membrane diffusion, thanks to the insertion of the acyl carrier protein (ACP) tag (or its shortened version S6 tag) at the extracellular receptor portion (Fig. 1A) and its specific conjugation to quantum dots (Qdots) [25], [27], [38]. We unveiled that NGF elicits a strong immobilization and clustering of membrane TrkA [24]. In order to unequivocally validate the relationship between membrane immobilization and receptor activation, we engineered an ACP-tagged construct in which Lys 547 (rat numbering, corresponding to human 544; Table S1) of *r*TrkA ATP-binding pocket was point-mutated to Asn (Fig. 1A). This substitution occurs in a conserved residue of the TKD N-lobe (Fig. 1A), and is a commonly adopted TrkA kinase-inactive variant (Table S1), while completely preserving NGF binding ability (Fig. S1). Both *r*TrkA-wt and -K547N were transfected in SHSY5Y cells, their membrane pool labelled with Qdots and imaged by TIRF with single-molecule resolution. Visual inspection of the moving spots (Video S1-S2) and relative trajectories (Fig.1B) suggested that *r*TrkA-K547N moves slower and explores smaller regions of the membrane compared to *r*TrkA-wt. This was confirmed by quantitative analysis of the diffusion coefficient (D) of mobile trajectories: *r*TrkA-K547N displays a bimodal distribution of D values similar to *r*TrkA-wt, but the faster population is slowed (peaked at 0.2 $\mu m^2/s$ versus 0.3 $\mu m^2/s$) and significantly decreased (Fig. S2A), matching with the rise of receptors moving at lower D (peaked at 0.005 $\mu m^2/s$ versus 0.013 $\mu m^2/s$, Fig. 1C). Furthermore, we classified the receptor modes of motion in immobile, confined and diffusive categories. We observed that the diffusive population of *r*TrkA-K547N is reduced by about 43% with respect to *r*TrkA-wt (Fig. 1D), matching with an increase of confined and immobile molecules. Thus, this specific lysine mutation alters receptor lateral mobility already in the absence of NGF stimulation. We then asked whether NGF binding

could change the dynamics of *r*TrkA-K547N, similarly to what observed for the wt counterpart [24], and accordingly analyzed by SPT the effect of 15 minutes NGF stimulation in the two cases. From the analysis of the D distributions, we verified that NGF-stimulated *r*TrkA-wt displays a significant slowdown and reduction of the fast-diffusing population (Figs. 1E and S2B) and a 34% increase of the immobile mode of motion (Fig. 1D and [24]). When analyzing the same for *r*TrkA-K547N, we again found a significant slowdown and reduction of fast-diffusing trajectories, but this was not as prominent as in the *r*TrkA-wt case (Figs.1E and S2B). Also, immobilization is less represented for *r*TrkA-K547N than for *r*TrkA-wt in the presence of NGF (Fig. 1D). We also calculated the distribution of confinement length for non-mobile trajectories [24] of *r*TrkA-K547N, observing no significant changes upon NGF stimulation, as instead we observed for the wt counterpart (Fig. 1F). These data indicate that NGF has an effect on *r*TrkA-K547N membrane dynamics, but with different features and weaker than on the *r*TrkA-wt one. Interestingly, we found that *r*TrkA-K547N displays a 3-fold higher surface density than *r*TrkA-wt; densitometric analysis of western blot from whole cell lysates suggests that this is not due to an increase of the total protein level (Fig.1G). We next investigated whether NGF has an effect in clearing this membrane accumulation, similarly to the internalization occurring for activated TrkA-wt [39], [40]. We set up a single-molecule internalization assay in which the density of membrane receptors of the two constructs was monitored by TIRF at eight time points within 60 minutes after NGF addition (Fig. 1H), and without NGF addition as control (Fig. S3). We found that *r*TrkA-wt and *r*TrkA-K547N decrease their membrane pool during time with different kinetics. For *r*TrkA-wt, the decrease starts at 5 min, becomes significant at 30 min and clearance of ~60% of the moving receptors from the cell membrane is accomplished after 40 minutes. On the contrary, *r*TrkA-K547N maintains a constant level of receptors exposed at the cell membrane up to 15 minutes after NGF

stimulation; this slightly decreases in the following but reaches a significant decrease of ~36% only after 50 minutes. These results suggest that *r*TrkA-K547N remains more time at the plasma membrane despite NGF stimulation, indicating an impairment of internalization for this mutant.

Given the high degree of conservation of this Lys residue in the ATP-binding pocket (Fig. 1A and [2]), our data hint at the existence of a general mechanism regulated by changes at this specific residue. Accordingly, the corresponding mutation introduced in *m*VEGFR2 (K866N corresponding to K868N in *h*VEGFR2, Table S2), abolished kinase activity, reduced membrane mobility and increased membrane pool when compared to *m*VEGFR2-wt (Fig. S4).

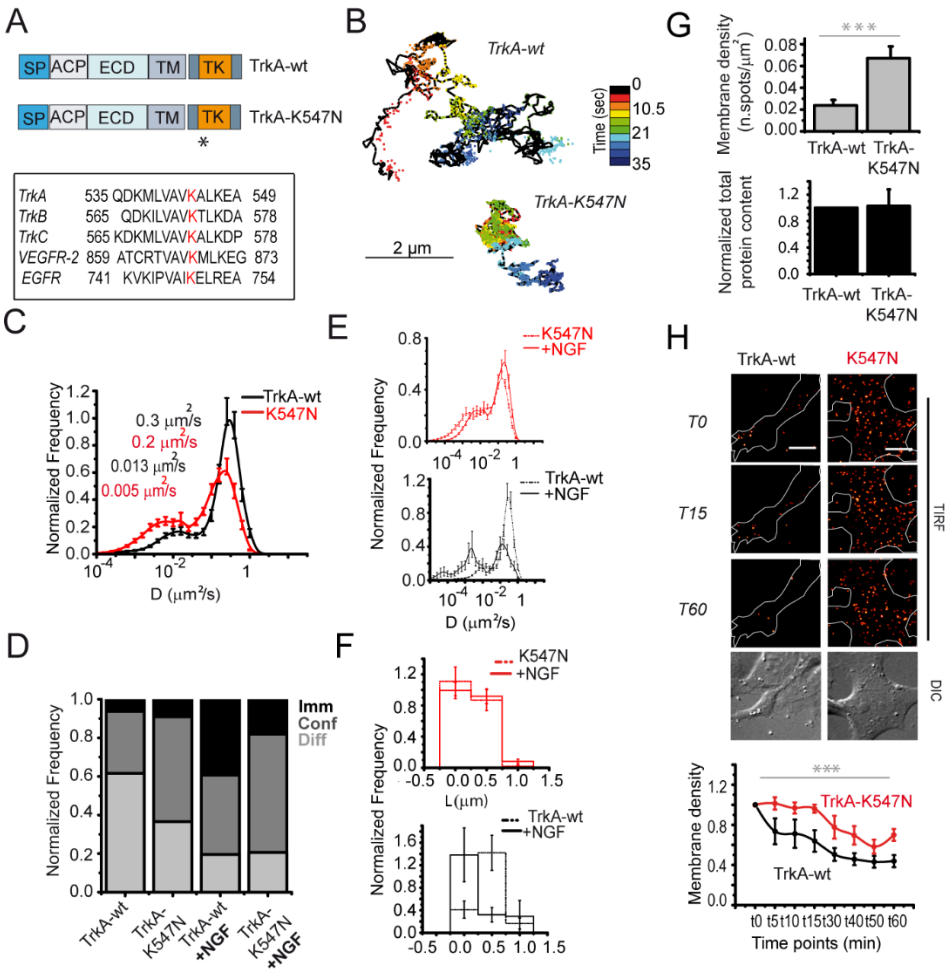

Fig. 1 Membrane immobilization and accumulation of *r*TrkA-K547N mutant. A) Scheme of *r*TrkA-wt and *r*TrkA-K547N (SP: signal peptide, ACP: acyl carrier protein tag, ECD: extracellular domain, TM: transmembrane domain, TK: Tyrosine Kinase domain); the asterisk highlights where the mutation is located. Below: sequence alignment of a portion of TKD for human sequences of TrkA, TrkB, TrkC, VEGFR2 and EGFR; the conserved Lys residue positioned in β3 sheet is shown in red. **B)** Typical trajectories obtained for moving *r*TrkA-wt (top) and -K547N (bottom) particles. **C)** Distribution of diffusion coefficient (D) with estimated uncertainty obtained from mobile *r*TrkA-wt (black curve, n=1989) and -K547N (red curve, n=1558) trajectories. **D)** Stack-column histogram plot of diffusive (light-grey), confined (grey) or immobile (black) receptors for *r*TrkA-wt without (n=2279 trajectories) and with NGF (n=513 trajectories), *r*TrkA-K547N without (n=2085 trajectories) and with NGF (n=2909 trajectories). The total number of trajectories was normalized to 1. **E)** Distribution of D coefficient with estimated uncertainty of mobile trajectories for *r*TrkA-K547N after NGF administration (top, red solid curve, n=2909 trajectories) and *r*TrkA-wt (bottom, black solid curve, n=529 trajectories); the D distribution of resting

*r*TrkA-K547N (red) and *r*TrkA-wt (black) are reported as dotted curve as a reference. **F)** Distributions of confinement length (L) with estimated error for non-mobile *r*TrkA-K547N (red) and *r*TrkA-wt (black) trajectories in the presence (solid; $n_{TrkA\text{-}K547N}$=616 and $n_{TrkA\text{-}wt}$=101 trajectories) or absence (dotted; $n_{TrkA\text{-}K547N}$=572 and $n_{TrkA\text{-}wt}$=290 trajectories) of NGF. p=0.38 (*r*TrkA-K547N) and p=4.9×10^{-4} (*r*TrkA-wt), according to χ^2 test. **G)** Density of labelled receptors per cell area (n=22 cells for *r*TrkA-wt, n=34 cells for *r*TrkA-K547N). ***p<0.0001 according to Mann-Whitney test. Below: densitometric analysis of total *r*TrkA-wt and *r*TrkA-K547N bands obtained averaging four independent blots; *r*TrkA-K547N signal was normalized to that of *r*TrkA-wt; error bars are standard errors. **H)** TIRF images of single receptor spots during a time-course after NGF stimulation. Cell borders are highlighted by a guide for the eye line. Every image corresponds to a time point for the same cell: t0 (time of NGF administration), t5, t15, t60 minutes. On the bottom, corresponding DIC image; scale bar=10 µm. The membrane density quantification for *r*TrkA-wt and *r*TrkA-K547N is reported as mean±sem from cells acquired at each time point normalized for the respective density at time 0. *** $p_{construct}$<0.001 and p_{time}<0.001, according to two-way ANOVA. All data are pools from up to 20 different cells collected in three independent replicas.

3.2 A structural rearrangement of the TKD correlates with *r*TrkA-K547N membrane immobilization

Mutation of Lys544 in *h*TrkA sequence (Lys547 in *r*TrkA) impairs kinase activity, recruitment of intracellular effectors and receptor ubiquitination [22], [23]. As impairment of any of these functions may potentially lead to the observed altered membrane dynamics (Fig. 1), we produced three additional *r*TrkA mutants to dissect the individual contributions to TrkA mobility. As reported in Fig. 2A, we generated: i) the Y499F/Y760F/Y794F mutant (recruitment mutant of *r*TrkA, RM); ii) the Y679F/Y683F/Y684F mutant (kinase mutant of *r*TrkA, KM); and iii) *r*TrkA-P791S mutant (ubiquitination mutant). The last one is modified in the binding site for the E3 Ubiquitin-ligase Nedd 4-2 [22]. This presumably accounts for the most abundant TrkA ubiquitination: indeed, differently from others, ubiquitination by Nedd 4-2 does not require overexpression of ubiquitin constructs to be detected [22], [23]. We

transfected RM, KM and *r*TrkA-P791S in SHSY5Y cells, and receptors were labelled to monitor their membrane dynamics by TIRF. Quantification of the obtained trajectories revealed that none of the compromised functions is responsible for *r*TrkA-K547N altered dynamics. Indeed, the modes of motion displayed by RM, KM, *r*TrkA-P791S were almost superimposable to those of *r*TrkA-wt (Fig. 2B).

It is well known that this mutated Lys (Fig. 1A) has a key structural role in the definition of a salt bridge linking strand β3, containing the Lys, to a Glu (563 in *r*TrkA and 560 in *h*TrkA) in the αC helix in the N lobe of TKD [43]. This salt bridge is highly conserved across different RTKs [2]. We thus hypothesized that the K→N mutation leads to a structural rearrangement of TrkA TKD that, independently of the functional impairment, may account for the observed entrapment in the membrane. This prompted us to perform molecular dynamics (MD) simulations of the *h*TrkA TKD in the wt configuration or after insertion of K544N mutation; we also simulated the behavior of a *h*TrkA-K544R mutant, in which the Arg possibly maintains the aforementioned salt bridge, while still compromising phosphorylation (Table S1). We focused on possible structural alterations induced by the K→N mutation. Surprisingly the MD simulations, while predicting a limited impact on strand β3, highlight a higher destabilization in the αC helix (Fig. 2C and Fig. S5C). This leads to distinct sub-populations characterized by different positioning of the αC helix with respect to strand β3 and C lobe, including one triggered by the formation of a new salt bridge between Glu560 in the αC helix and Arg673, located between β8 and β9 (Fig.2D and Fig. S5A). This effect is strictly dependent on the lack of Lys544-Glu560 salt bridge: indeed, substitution of Lys544 with salt-bridge preserving Arg (Fig. 2C-D) maintains the stability of the αC helix in the MD simulations (Fig. 2C and Fig. S4B). Conversely, two different but both salt-bridge abolishing amino acids like Ala or Pro are

predicted to destabilize the αC helix (Fig. S4B-C). These results prompted us to express and Qdot-label an ACP-tagged *r*TrkA-K547R in SHSY5Y cells; we found that, although this mutant is not phosphorylated, its membrane dynamics is more similar to that of *r*TrkA-wt than of *r*TrkA-K547N (Fig. 3A-B and Fig. S6). Thus, the K→N mutation in β3-sheet is predicted to yield specific structural rearrangements; a possible consequence of these could be an aggregation of the TKDs that may favor the formation of receptor homo-clusters with the consequent decrease in the measured diffusion. Indeed, TrkA crystal structure already showed the possibility to form dimers and probably oligomers in the crystal unit [29]. To test this hypothesis, we analyzed the intensity step-photobleaching profile of *h*TrkA-wt, *h*TrkA-K544N and *h*TrkA-K544R single molecules in the membrane of fixed cells (red boxes of Fig. 3C). For each spot, we quantified the number of photobleaching steps as a direct measure of the number of molecules in an isolated spot [28]. The results highlight no significant changes in the monomer, dimer and oligomer populations in the three cases (M, D, O in Fig. 3D, respectively), thus ruling out the possibility of increased homo-aggregation as the molecular cause for the observed *h*TrkA-K544N membrane dynamics.

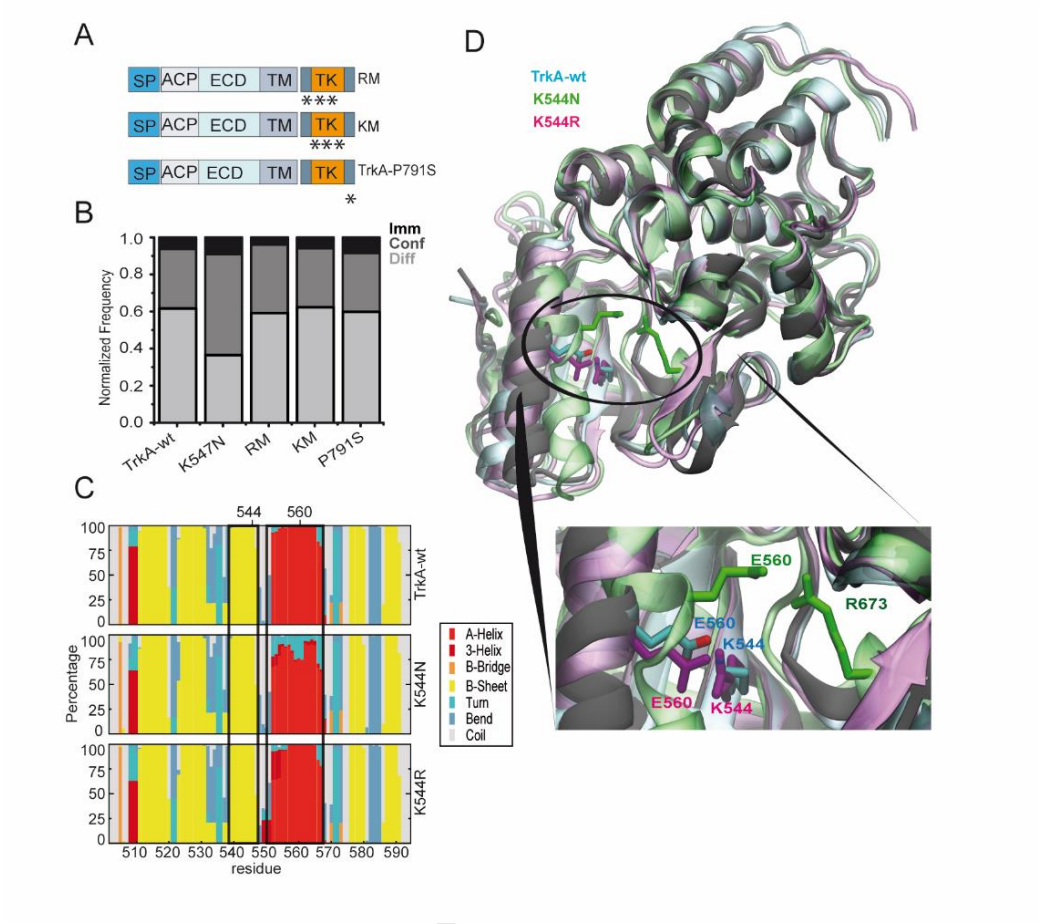

Fig. 2 A structural change of the TKD correlates with *r*TrkA-K547N membrane immobilization. A) Scheme of recruitment mutant (RM), kinase mutant (KM) and ubiquitination mutant (*r*TrkA-P791S). SP: signal peptide, ACP: acyl carrier protein tag, ECD: extracellular domain, TM: transmembrane domain, TK: Tyrosine Kinase domain; asterisks highlight the positions of the single mutations in the intracellular region (Y to F in RM and KM). **B)** Stack-column histogram plot for diffusive (light-grey), confined (grey), immobile (black) receptors obtained for *r*TrkA mutants. The total number of trajectories (RM: n=6638, KM: n=7777 and *r*TrkA-P791S: n=1841 trajectories; *r*TrkA-wt and *r*TrkA-K547N of Fig. 1D are here reported as a reference) was normalized to 1. All data are pools from up to 20 different cells collected in three independent replicas. **C)** MD analysis of secondary structure elements encompassing residues 501 to 593 in *h*TrkA-wt (top), *h*TrkA-K544N (middle) and *h*TrkA-K544R (bottom). The regions corresponding to the αC helix and the β3 sheet are highlighted by a black rectangle. **D)** Selected snapshots from MD simulations of *h*TrkA-wt TKD (cyan), and its K544N (green) and K544R (magenta) mutants superimposed on the *h*TrkA-wt TKD crystal structure (PDB: 4f0i, gray).

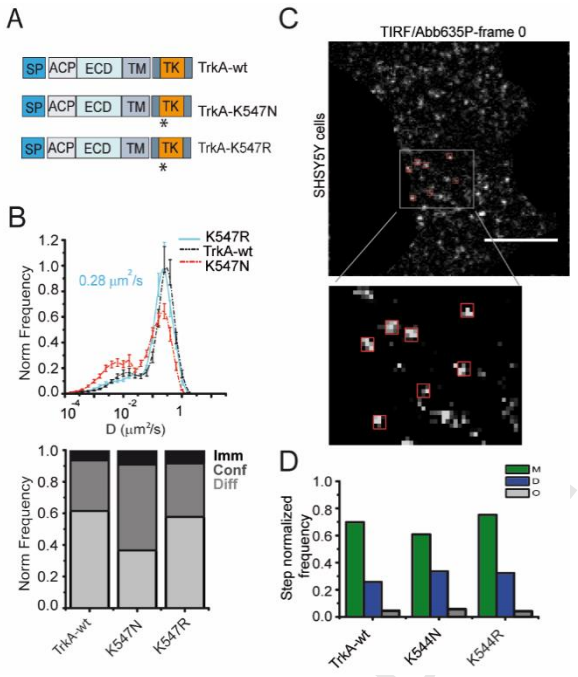

Fig. 3 *r*TrkA-K547N membrane immobilization depends on the lack of Lys-Glu salt bridge but not on increased receptor homo-aggregation. A) Scheme of *r*TrkA-wt, *r*TrkA-K547N and *r*TrkA-K547R (SP: signal peptide, ACP: acyl carrier protein tag, ECD: extracellular domain, TM: transmembrane domain, TK: Tyrosine Kinase domain); the asterisk highlights where the single point mutations are located. **B)** Top: distribution of diffusion coefficient (D) with estimated uncertainty obtained for mobile *r*TrkA-K547R trajectories (dark cyan curve, n=936). Bottom: stack-column histogram plot of diffusive (light grey), confined (grey), immobile (black) receptors obtained for *r*TrkA-K547R (1745 trajectories), *r*TrkA-wt and *r*TrkA-K547N (same data of Fig. 1D). **C)** TIRF image of Abberior635P-labelled *h*TrkA spots on the surface of fixed SHSY5Y cells: red squares in the inset are the 3×3 pixels ROI highlighting the analyzed spots in the first frame of the background-subtracted TIRF movie. **D)** Frequency of photobleaching steps (M=1 step; D=2 steps; O= at least 3 steps) counted for *h*TrkA-wt (n=245 spots), *h*TrkA-K544N (n=286 spots) and *h*TrkA-K544R (n=355 spots); differences are not significant according to χ^2 test. All data are pools from 10 to 19 different cells collected in three (B) and two (D) independent replicas.

3.4 *r*TrkA-K547N membrane mobility depends on the integrity of cortical actin

We next investigated if the altered membrane mobility of *r*TrkA-K547N could be due to new hetero-interactions maintaining the structurally rearranged receptor within different membrane domains than *r*TrkA-wt. As micro- and nano- domains in the plasma membrane are structured by fences of cortical actin, which confine in space and time the diffusivity of transmembrane

receptors [42], [43], we treated cells with drugs affecting the polymerization state of actin, either by disrupting (cytochalasin D, latrunculin B) or by stabilizing (jasplakinolide) actin fibers integrity, as evidenced by phalloidin staining of the cells after the treatment (Fig. 4A). By performing SPT measures in these conditions, we found that the *r*TrkA-K547N confined and immobile modes of motion were substantially impaired by actin depolymerization (Fig. 4C), as was the accumulation of surface *r*TrkA-K547N receptors (Fig. 4B, D); the latter turned out to slightly increase when we stabilized the polymerized form of actin fibers (Fig. 4B-D). The same treatments tested on *r*TrkA-wt showed an opposite trend in the modes of motion after actin depolymerization (Fig. 4E), and no significant effect on the density of surface receptors (Fig. 4B, F). These data suggest that *r*TrkA-K547N, but not *r*TrkA-wt, is either stably entrapped within membrane regions maintained by the actin meshwork, or directly interacts with it, justifying the specific slow membrane dynamics and the surface accumulation displayed by this mutant.

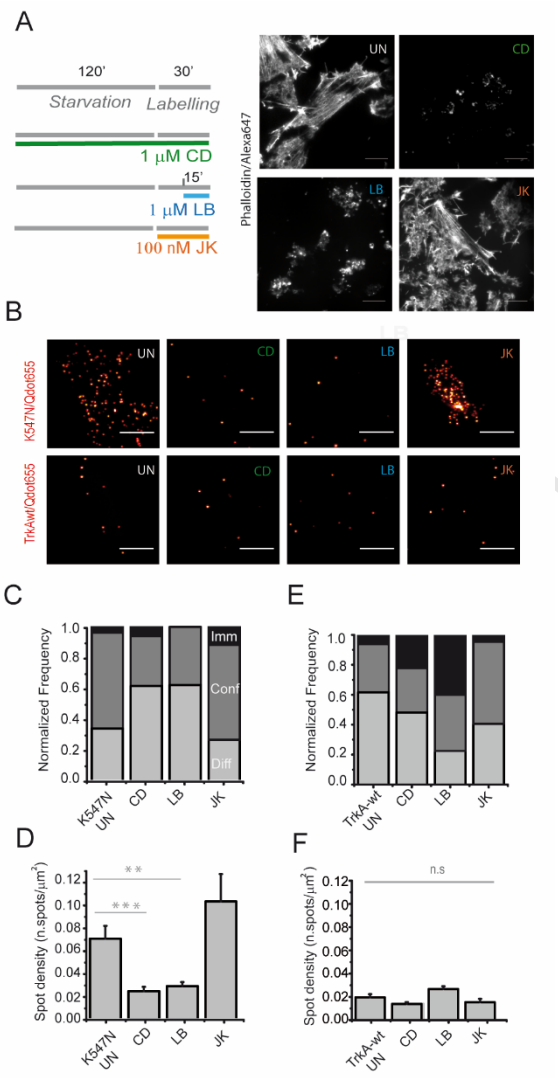

Fig. 4 Actin cytoskeleton mediates membrane immobilization and accumulation of *r*TrkA-K547N. A) Left: Timeline of the SPT experiment on *r*TrkA-K547N and *r*TrkA-wt in the presence of drugs affecting actin polymerization. CD: Cytochalasin D; LB: Latrunculin B; JK: Jasplakinolide**;** right: typical TIRF images of SHSY5Y cells labelled with Alexa647-phalloidin after the treatments (UN: untreated). Scale bar: 10 μm. **B)** TIRF images of *r*TrkA-K547N (top) and *r*TrkA-wt (bottom) transfected SHSY5Y cells after Qdot labeling, in untreated and CD-, LB- and JK- treated conditions. Scale bar=10 μm. **C)** Stack-column histogram plot for the distribution of diffusive (light grey), confined (grey) and immobile (black) *r*TrkA-K547N receptors in untreated conditions (same as Fig. 1E) and after CD, LB, JK treatments (CD, n=904; LB, n=366; JK, n=1606 trajectories). **D)** *r*TrkA-K547N surface density in untreated conditions and after CD, LB, JK treatments (untreated, n=22; CD= 15; LB=17; JK= 23 cells). ***p<0.001, **p <0.01 according to Kruskal-Wallis test followed by Dunn's Multiple Comparison test. **E)** Stack-

column histogram plot for the distribution of diffusive (light grey), confined (grey) and immobile (black) *r*TrkA-wt receptors in resting conditions (same as Fig. 1E) and in the presence of CD, LB, JK drugs (CD: n=169; LB: n= 169; JK: n=100 trajectories). **F)** *r*TrkA-wt surface density in untreated conditions and after CD, LB, JK treatments (untreated, n=10 cells; CD= 7 cells; LB=8 cells; JK= 6 cells). Differences are not significant according to Kruskal-Wallis test followed by Dunn's Multiple Comparison test. SPT data are pools from up to 23 different cells collected in three independent replicas.

3.5 Contribution of PTMs on NGF-induced TrkA membrane immobilization

From data reported in Fig. 1D-F, we concluded that *r*TrkA-wt displays a remarkably higher membrane immobilization induced by NGF stimulation, when compared to *r*TrkA-K547N. Given that ligand-induced immobilization was correlated to RTKs activation [24], [44], we aimed at understanding which functional feature is responsible for it. Biochemical analysis of *r*TrkA-K547N, RM, KM, *r*TrkA-P791S in comparison to *r*TrkA-wt revealed that NGF-induced phosphorylation and ubiquitination could be fully dissected by using these mutants. As shown in Fig. 5A, only *r*TrkA-wt showed significant phosphorylation and ubiquitination signals upon NGF stimulation; *r*TrkA-P791S was significantly phosphorylated but not ubiquitinated; TrkA-K547N was significantly ubiquitinated but not phosphorylated; RM and KM did not display significant levels of either PTM (Fig. 5A). We thus performed SPT analysis for RM, KM and *r*TrkA-P791S in the presence of NGF, as already done for *r*TrkA-wt and *r*TrkA-K547N (Fig. 1D-F), and calculated the variation of the modes of motion of all constructs after NGF stimulation. Interestingly, we found that all TrkA mutants investigated display weaker NGF-induced immobilization than *r*TrkA-wt (Fig. 5B), meaning that this effect conceivably requires both unaltered phosphorylation and ubiquitination to occur.

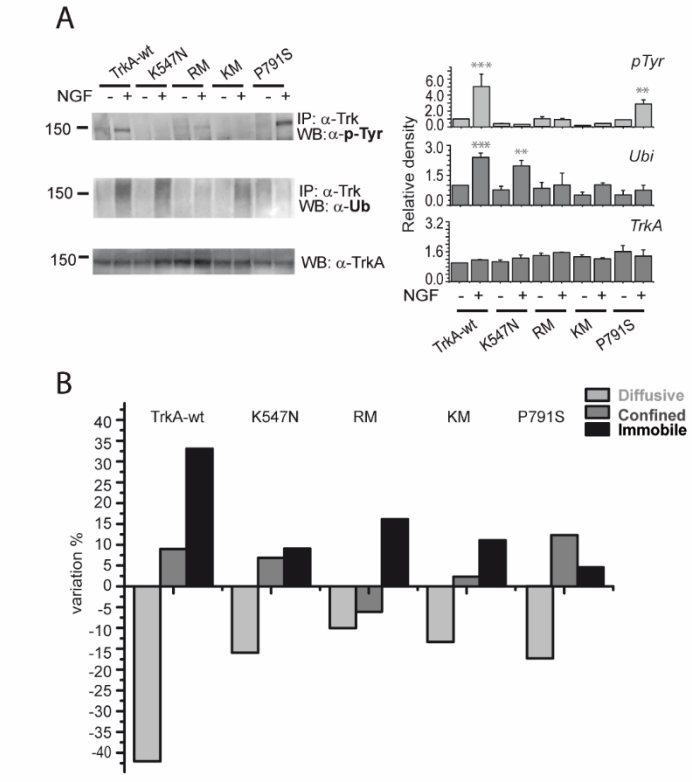

Fig.5 Impact of PTMs on NGF-induced TrkA membrane dynamics. A) WB showing Tyr phosphorylation (p-Tyr, top) and ubiquitin (Ub, middle) levels in SHSY5Y cells transfected with *r*TrkA-wt, *r*TrkA-K547N, RM, KM, *r*TrkA-P791S in the presence (+) or absence (-) of 10 minutes stimulation with 125 ng/ml NGF, after immunoprecipitation (IP) with anti-Trk antibody. The relative density of the bands is reported on the right of each blot, as mean±sem of 2-5 independent replicas; each band density was normalized to the total TrkA content obtained after membrane stripping, and divided for *r*TrkA-wt value (p-Tyr Blot: n=3 for all constructs; Ub blot: n=5, *r*TrkA-wt; n=4, *r*TrkA-K547N; n=2, RM; n=3, KM, *r*TrkA-P791S). ***p<0.001, **p<0.01, according to one-way Anova with Bonferroni's multiple comparison test. Bottom: WB showing total TrkA levels for the same samples as above. The relative density of the bands is reported on the right of the blot, as mean±sem of 3 independent replicas; the band density was normalized to the total protein content of each lane (Fig. S7), and divided for TrkA-wt value. Data are not significantly different according to one-way Anova with Bonferroni's multiple comparison test. **B)** Column plot of the variation (in percentage of the total) of diffusive (light-grey), confined (grey), immobile (black) receptor populations upon NGF stimulation for *r*TrkA-wt (n=513), *r*TrkA-K547N (n=2909), RM (n= 531), KM (n=1848) and *r*TrkA-P791S (n=1526 trajectories); the number of trajectories

analyzed in resting conditions for each mutant are reported in Fig.2B. All trajectories are pools from up to 20 cells from three independent replicas.

4. Discussion

We previously demonstrated that TrkA membrane mobility measured by TIRF microscopy combined with SPT is highly predictive of its function, with immobilization and clustering being a signature of the activating ligand [24]. This ligand-dependent effect agrees with similar results reported for EGFR [44], FLS2 receptor-like kinase [45] and insulin receptor kinase [46]. Overall, these works have allowed for the definition of a direct cause-effect relationship between RTKs activation and immobilization of their membrane pool. Here, we scale-up our study by analyzing different TrkA mutants in comparison to TrkA-wt, and provide evidence that such relation may be more complicated than expected. Indeed, our results show that it is possible to distinguish at least two different TrkA membrane immobilization modes. On one hand, K544N mutation (in *h*TrkA corresponding to K547N in *r*TrkA, Table S1) in sheet β3 of TrkA TKD endows the receptor with increased confined and immobile membrane fractions with respect to TrkA-wt, independently of NGF binding (Fig. 1C-F), and with an enrichment of surface pool (Fig. 1G). The importance of these observations is strengthened by evidence that at least another RTK, VEGFR2, shares similar features upon mutation of the corresponding Lys to Asn (Figs. 1A, S4 and S5). Mutations of these Lys residues were previously adopted as kinase-dead variants of TrkA and VEGFR2 receptors (Tables S1-2), since they impair ATP allocation necessary to TKD activation and downstream phosphorylation processes [47]. Furthermore, mutation of this residue was previously linked to impaired ubiquitination [22], [23]. However, we argue that the altered membrane mobility does not singularly depend on TrkA kinase activity, on its ability to recruit intracellular

effectors at phosphorylated Tyr, nor on its ubiquitination; indeed, mutants in which these functions are separately impaired do not show the same slowdown in the detected trajectories (KM, RM and *r*TrkA-P791S in Fig. 2B). Instead, our MD simulations indicate that, in *h*TrkA-K544N, the αC helix of the N lobe becomes less stable as a consequence of the loss of a salt bridge with β3 sheet (Fig. 2C-D), and can adopt different arrangements with respect to the C lobe (Fig. 2C-D and S5). *r*TrkA-K547R, a kinase-inactive mutant that maintains the salt bridge, does not display the repositioning of the αC helix (Fig. 2C-D) and does not show altered modes of motion in the analyzed trajectories with respect to *r*TrkA-wt (Fig. 3A-B). Based on results in Figs. 3-4, we hypothesize that these structural changes do not increase the propensity of the receptor to self-aggregate, but rather could account for new hetero-interactions leading to the observed confinement and immobilization at the cell surface detected by SPT. On the other hand, a different membrane immobilization is experienced by *r*TrkA-wt, at higher extent than *r*TrkA-K547N, after NGF stimulation, with D and L distributions changing considerably in the wt but not in the K547N case (Fig. 1E-F) and with less represented decrease of diffusive trajectories for TrkA-K547N (Fig. 1D). In this respect, it is noteworthy that all TrkA mutants assessed by SPT show impaired NGF-induced membrane immobilization (Fig. 5B), despite their conserved ability to bind NGF (Fig. S1). Both NGF-induced TrkA phosphorylation and ubiquitination account for it. We thus speculate that the shared tendency of all analyzed mutants to undergo only small reductions of diffusivity may simply be due to NGF binding to their ECD. This, while possibly inducing their dimerization, may not result in the robust and signaling-related immobilization typical of the wt receptor.

The lateral diffusivity of membrane proteins and lipids is modulated by the presence of specialized physical barriers [48] like actin fences [49]. These fibers, lying in close contact with the inner leaflet of the plasma membrane, can constrain transmembrane proteins within

transient confinement regions called corrals [50]. The slow dynamic profile reported for *r*TrkA-K547N can be reliably ascribed to interactions with these membrane regions. Indeed, cortical-actin depolymerization (Fig. 4A) leads to an accelerated diffusion and decreased accumulation of *r*TrkA-K547N (Fig. 4B-C-D). The same drug treatments lead to opposite changes for *r*TrkA-wt, (Fig. 4B-E-F and [24]). These data indicate different dynamic interactions of *r*TrkA-wt and *r*TrkA-K547N with the actin cytoskeleton, which might be relevant for the different signaling abilities displayed by the two receptor forms. However, whether an enhanced partitioning within the aforementioned domains or direct interactions with actin account for *r*TrkA-K547N slow membrane dynamics remains to be established.

TrkA has been reported to be ubiquitinated, in different experimental conditions, by a number of different E3-ubiquitin ligases, namely TRAF-6 E3 RING Ub-ligase [51], Nedd 4-2 E3 HECT Ub-ligase [22], [52], TRAF-4 E3 RING Ub-ligase [23], and Cbl [53]. This prompted us to investigate whether this PTM plays a role also in TrkA membrane dynamics. We found that *r*TrkA-K547N can be significantly ubiquitinated after NGF treatment (Fig. 5 A) in SHSY5Y cells, while lysine 547 mutation leads to impairment of TrkA ubiquitination in HEK293 cells in the absence of NGF [22]. However, we found that NGF addition may restore ubiquitination of different lysine 547 mutants in this cell model (Fig. S8A). Also, *r*TrkA-wt is equally ubiquitinated in resting and NGF-stimulated conditions in HEK293 cells. This may be due to a higher expression level of the construct than in SHSY5Y cells, leading to ligand-independent auto-activation (Fig. S8A). Alternatively, possible differential regulatory patterns on TrkA could be driven by different cell backgrounds. In this context, it should be noted that both *r*TrkA-wt and *r*TrkA-K547N proteins show different mobilities in HEK293 when compared to SHSY5Y cells (Fig. 1C and S8B). In any case, the observation that inhibition of *r*TrkA ubiquitination by the P791S mutation, without perturbing kinase activity (Fig. 5A), is sufficient to impair NGF-

induced immobilization of *r*TrkA-wt (Fig. 5B) suggests that this PTM plays a crucial role in the regulation of its membrane dynamics.

5. Conclusions

The findings emerging from our study enrich our knowledge of RTKs, but also unavoidably call into question the interpretation of previous experiments indifferently making use of distinct mutations to achieve abolition of RTK kinase activity (Tables S1 and S2). Indeed, our data indicate that not all kinase-inactive TrkA mutants behave in the same way, at least concerning membrane mobility (Figs. 1-3) and ubiquitination (Fig. 5). Furthermore, our data also suggest that understanding the effect of a TKD mutation may benefit from analysis of its impact on the KD structure, in addition to catalytic activity. This may be useful to understand the molecular basis of pathogenicity of the several inactivating mutations disseminated along TrkA, and more in general RTKs, sequence.

Acknowledgments

The authors wish to gratefully thank A. Cattaneo and F. Beltram for helpful discussions, F. Bonsignore, F. Gobbo and L. Ceccarelli for technical help, G. Signore for making CoA-biotin reagent available, and G. Ferri for help with MATLAB codes. Grant AIRC IG17276 to SM is gratefully acknowledged. The authors declare no competing financial interests.

References

[1] M. A. Lemmon and J. Schlessinger, “Cell signaling by receptor tyrosine kinases,” *Cell*, vol. 141, no. 7, pp. 1117–1134, 2010.

[2] J. M. M. Mendrola, F. Shi, J. H. H. Park, and M. A. A. Lemmon, “Receptor tyrosine kinases with intracellular pseudokinase domains,” *Biochem. Soc. Trans.*, vol. 41, no. 4, pp. 1029–1036, Aug. 2013.

[3] B. Nolen, S. Taylor, and G. Ghosh, “Regulation of protein kinases: Controlling activity through activation segment conformation,” *Mol. Cell*, vol. 15, no. 5, pp. 661–675, 2004.

[4] P. Blume-Jensen and T. Hunter, “Oncogenic kinase signalling : Abstract : Nature,” *Nature*, vol. 411, no. 6835, pp. 355–365, 2001.

[5] G. Giamas *et al.*, “Kinases as targets in the treatment of solid tumors,” *Cell. Signal.*, vol. 22, no. 7, pp. 984–1002, 2010.

[6] L. M. McDonell, K. D. Kernohan, K. M. Boycott, and S. L. Sawyer, “Receptor tyrosine kinase mutations in developmental syndromes and cancer: Two sides of the same coin,” *Hum. Mol. Genet.*, vol. 24, no. R1, pp. R60–R66, 2015.

[7] S. C. Robertson, J. A. Tynan, and D. J. Donoghue, “RTK mutations and human syndromes - When good receptors turn bad,” *Trends Genet.*, vol. 16, no. 6, pp. 265–271, 2000.

[8] M. Odawara *et al.*, “Human Diabetes Associated with a Mutation in the Tyrosine Kinase Domain of the Insulin Receptor Akanuma , Fumimaro Takaku , Simeon I . Taylor and Masato Kasuga Published by : American Association for the Advancement of Science Stable URL : http://www.jsto,” 2016.

[9] K. A. E. Stenberg, P. T. Riikonen, and M. Vihinen, “KinMutBase, a database of human disease-causing protein kinase mutations,” *Nucleic Acids Res.*, vol. 27, no. 1, pp. 362–364, 1999.

[10] J. Boudeau, D. Miranda-Saavedra, G. J. Barton, and D. R. Alessi, “Emerging roles of pseudokinases,” *Trends in Cell Biology*. 2006.

[11] M. V. Chao, “Neurotrophins and their receptors: A convergence point for many signalling pathways,” *Nat. Rev. Neurosci.*, vol. 4, no. 4, pp. 299–309, 2003.

[12] A. W. Harrington and D. D. Ginty, “Long-distance retrograde neurotrophic factor signalling in neurons,” vol. 14, no. March, pp. 177–187, 2013.

[13] A. Vaishnavi, A. T. Le, and R. C. Doebele, “TRKing down an old oncogene in a new era of targeted therapy,” *Cancer Discovery*. 2015.

[14] S. Capsoni, “From genes to pain: nerve growth factor and hereditary sensory and autonomic neuropathy type V,” *Eur. J. Neurosci.*, 2014.

[15] S. R. Hubbard, “Structural analysis of receptor tyrosine kinases,” *Prog. Biophys. Mol. Biol.*, vol. 71, no. 3–4, pp. 343–358, 1999.

[16] I. Maruyama, “Mechanisms of Activation of Receptor Tyrosine Kinases: Monomers or Dimers,” *Cells*, vol. 3, no. 2, pp. 304–330, 2014.

[17] M. E. Cunningham and L. A. Greene, “A function – structure model for NGF-activated TRK,” vol. 17, no. 24, pp. 7282–7293, 1998.

[18] R. A. Segal *et al.*, “Differential utilization of Trk autophosphorylation sites,” *J. Biol. Chem.*, vol. 271, no. 33, pp. 20175–20181, 1996.

[19] J. Biarc, R. J. Chalkley, A. L. Burlingame, and R. A. Bradshaw, “Dissecting the roles of tyrosines 490 and 785 of TrkA protein in the induction of downstream protein phosphorylation using chimeric receptors,” *J. Biol. Chem.*, vol. 288, no. 23, pp. 16606–16618, 2013.

[20] N. Inagaki, H. Thoenen, and D. Lindholm, “TrkA Tyrosine Residues Involved in NGF-induced Neurite Outgrowth of PC12 Cells,” *Eur. J. Neurosci.*, vol. 7, no. 6, pp. 1125–1133, 1995.

[21] A. Obermeier, H. Halfter, K. H. Wiesmüller, G. Jung, J. Schlessinger, and A. Ullrich,

"Tyrosine 785 is a major determinant of Trk--substrate interaction.," *EMBO J.*, vol. 12, no. 3, pp. 933–41, 1993.

[22] J. C. Arévalo *et al.*, "Cell Survival through Trk Neurotrophin Receptors Is Differentially Regulated by Ubiquitination," *Neuron*, vol. 50, no. 4, pp. 549–559, 2006.

[23] R. Singh *et al.*, "TRAF4-mediated ubiquitination of NGF receptor TrkA regulates prostate cancer metastasis," *J. Clin. Invest.*, vol. 128, no. 7, pp. 3129–3143, 2018.

[24] L. Marchetti *et al.*, "Ligand signature in the membrane dynamics of single TrkA receptor molecules," *J. Cell Sci.*, vol. 126, no. 19, pp. 4445–4456, 2013.

[25] A. Callegari, S. Luin, L. Marchetti, A. Duci, A. Cattaneo, and F. Beltram, "Single particle tracking of acyl carrier protein (ACP)-tagged TrkA receptors in PC12nnr5 cells," *J. Neurosci. Methods*, vol. 204, no. 1, pp. 82–86, 2012.

[26] L. Marchetti *et al.*, "Site-specific labeling of neurotrophins and their receptors via short and versatile peptide tags," *PLoS One*, vol. 9, no. 11, pp. 1–18, 2014.

[27] F. Gobbo, F. Bonsignore, R. Amodeo, A. Cattaneo, and L. Marchetti, "Site-specific direct labeling of neurotrophins and their receptors: From biochemistry to advanced imaging applications," in *Methods in Molecular Biology*, vol. 1727, 2018, pp. 295–314.

[28] L. Marchetti *et al.*, " Fast-diffusing p75 NTR monomers support apoptosis and growth cone collapse by neurotrophin ligands ," *Proc. Natl. Acad. Sci.*, 2019.

[29] T. Bertrand *et al.*, "The Crystal Structures of TrkA and TrkB Suggest Key Regions for Achieving Selective Inhibition," *J. Mol. Biol.*, vol. 423, no. 3, pp. 439–453, 2012.

[30] J. G. Kettle *et al.*, "Discovery of N-(4-{[5-Fluoro-7-(2-methoxyethoxy)quinazolin-4-yl]amino}phenyl)-2-[4-(propan-2-yl)-1 H-1,2,3-triazol-1-yl]acetamide (AZD3229), a Potent Pan-KIT Mutant Inhibitor for the Treatment of Gastrointestinal Stromal Tumors," *J. Med. Chem.*, vol. 61, no. 19, pp. 8797–8810, 2018.

[31] J. M. Word *et al.*, “Visualizing and quantifying molecular goodness-of-fit: Small-probe contact dots with explicit hydrogen atoms,” *J. Mol. Biol.*, vol. 285, no. 4, pp. 1711–1733, 1999.

[32] G. Vriend, “WHAT IF: A molecular modeling and drug design program,” *J. Mol. Graph.*, 1990.

[33] S. J. Fleishman *et al.*, “of Influenza Hemagglutinin,” *Science (80-.).*, vol. 979, no. May, pp. 816–822, 2011.

[34] K. Lindorff-Larsen *et al.*, “Improved side-chain torsion potentials for the Amber ff99SB protein force field,” *Proteins Struct. Funct. Bioinforma.*, vol. 78, no. 8, pp. 1950–1958, 2010.

[35] R. B. Best and G. Hummer, “Optimized molecular dynamics force fields applied to the helix-coil transition of polypeptides,” *J. Phys. Chem. B*, 2009.

[36] M. J. Abraham *et al.*, “Gromacs: High performance molecular simulations through multi-level parallelism from laptops to supercomputers,” *SoftwareX*, vol. 1–2, pp. 19–25, 2015.

[37] N. D. Gagunashvili, “Chi-square goodness of fit tests for weighted histograms. Review and improvements,” *J. Instrum.*, vol. 10, no. 5, 2015.

[38] L. Marchetti, S. Luin, F. Bonsignore, T. de Nadai, F. Beltram, and A. Cattaneo, “Ligand-induced dynamics of neurotrophin receptors investigated by single-molecule imaging approaches,” *Int. J. Mol. Sci.*, vol. 16, no. 1, pp. 1949–1979, 2015.

[39] E. C. Beattie, “NGF signals through TrkA to increase clathrin at the plasma membrane and enhance clathrin-mediated membrane trafficking.,” *J. Neurosci.*, vol. 20, no. 19, pp. 7325–7333, 2000.

[40] A. Disanza, E. Frittoli, A. Palamidessi, and G. Scita, “Endocytosis and spatial restriction

of cell signaling," *Mol. Oncol.*, vol. 3, no. 4, pp. 280–296, 2009.

[41] C. Wiesmann, M. H. Ultsch, and S. H. Bass, "Nature, 1999, 401, 184.pdf," vol. 401, no. SEPTEMBER, pp. 1–5, 1999.

[42] J. B. Casaletto and A. I. McClatchey, "Spatial regulation of receptor tyrosine kinases in development and cancer," *Nature Reviews Cancer*. 2012.

[43] A. Kusumi and Y. Sako, "Cell surface organization by the membrane skeleton Akihiro Kusumi * and Yasushi Sakot," *Cell*, vol. 8, no. 4, pp. 566–574, 1996.

[44] I. Chung, R. Akita, R. Vandlen, D. Toomre, J. Schlessinger, and I. Mellman, "Spatial control of EGF receptor activation by reversible dimerization on living cells.," *Nature*, 2010.

[45] G. S. Ali, K. V. S. K. Prasad, I. Day, and A. S. N. Reddy, "Ligand-dependent reduction in the membrane mobility of Flagellin sensitive2, an Arabidopsis receptor-like kinase," *Plant Cell Physiol.*, vol. 48, no. 11, pp. 1601–1611, 2007.

[46] P. W. Winter, A. K. Van Orden, D. A. Roess, and B. G. Barisas, "Actin-dependent clustering of insulin receptors in membrane microdomains," *Biochim. Biophys. Acta - Biomembr.*, vol. 1818, no. 3, pp. 467–473, 2012.

[47] A. C. Carrera, K. Alexandrov, and T. M. Roberts, "The conserved lysine of the catalytic domain of protein kinases is actively involved in the phosphotransfer reaction and not required for anchoring ATP.," *Proc. Natl. Acad. Sci.*, vol. 90, no. 2, pp. 442–446, 1993.

[48] A. Kusumi, K. G. N. Suzuki, R. S. Kasai, K. Ritchie, and T. K. Fujiwara, "Hierarchical mesoscale domain organization of the plasma membrane," *Trends Biochem. Sci.*, vol. 36, no. 11, pp. 604–615, 2011.

[49] W. S. Trimble and S. Grinstein, "Barriers to the free diffusion of proteins and lipids in the plasma membrane," *J. Cell Biol.*, vol. 208, no. 3, pp. 259–271, 2015.

[50] K. G. N. Suzuki, T. K. Fujiwara, F. Sanematsu, R. Iino, M. Edidin, and A. Kusumi, “GPI-anchored receptor clusters transiently recruit Lyn and G?? for temporary cluster immobilization and Lyn activation: Single-molecule tracking study 1,” *J. Cell Biol.*, vol. 177, no. 4, pp. 717–730, 2007.

[51] T. Geetha, J. Jiang, and M. W. Wooten, “Lysine 63 polyubiquitination of the nerve growth factor receptor TrkA directs internalization and signaling,” *Mol. Cell*, vol. 20, no. 2, pp. 301–312, 2005.

[52] T. Yu *et al.*, “In Vivo Regulation of NGF-Mediated Functions by Nedd4-2 Ubiquitination of TrkA,” *J. Neurosci.*, vol. 34, no. 17, pp. 6098–6106, 2014.

[53] Y. Takahashi *et al.*, “Ligand-induced downregulation of TrkA is partly regulated through ubiquitination by Cbl,” *FEBS Lett.*, vol. 585, no. 12, pp. 1741–1747, 2011.

Highlights

- K544N mutation causes reduced membrane mobility of unstimulated TrkA receptor
- Molecular dynamics simulations predict structural changes in mutated kinase domain
- Post-translational modifications drive membrane immobilization of NGF-bound TrkA
- Two distinct modes of TrkA membrane immobilization can be distinguished
- Not all kinase-inactive TrkA mutants display identical membrane trafficking

Supplementary methods

Cell culture, transfection and transduction

SHSY5Y (a kind gift from Fondazione EBRI, Rome, Italy) cells were grown in DMEM/F-12 medium supplemented with 10% Fetal Bovine Serum (FBS), 1% Penicillin-Streptomycin and 1% L-Glutamine and 25 mM HEPES. HEK293T/17 cells (ATCC® CRL-11268™) were grown in DMEM High-Glucose (4.5 g/L) medium supplemented with 10% Fetal Bovine Serum, 1% Penicillin-Streptomycin, 1% L-Glutamine, 1% Sodium Pyruvate. Fetal bovine aortic endothelial GM7373 cells [1] were grown in DMEM (Gibco, Life Technologies) containing 10% FBS, vitamins, essential and non-essential amino acids. GM7373 cells were transfected with a pcDNA3.1 expression vector harboring the wt and mutated forms of *m*VEGFR2 cDNA to generate stable GM7373-VEGFR2 transfectants. Transfections were performed by using the Lipofectamine™ 2000 reagent (Thermo Fisher Scientific), according to the manufacturer's instructions. Transduction of *h*TrkA-wt, *h*TrkA-K544N and *h*TrkA-K544R in SHSY5Y was performed as previously described [2]. Briefly, HEK293T cells were transfected using Effectene (Qiagen) and incubated at 37°C ON. The following day the medium was refreshed. After 24 hours we harvested culture medium containing virus-like particles (VLPs) and concentrated them with Lenti-X™ Concentrator (Clontech) ON at 4 °C; we repeated the harvest of VLPs after hours 48 and concentrated them for 1 h at 4 °C. After centrifugation we resuspended the obtained pellet in PBS with a 100x concentrated volume with respect to the initial medium volume. We then infected SHSY5Y cells seeded in a 30-mm-diameter culture dishes with 35 µl of viral stock diluted in 300 µl medium plus 0.4 ug/ml polybrene and incubated them at 37°C for 1 hour. After we replaced infection medium with complete culture medium, we incubated cells for 48 hours to allow transgene integration. Construct expression was induced by direct addition of 1 µg/ml Doxycicline to the culture medium. After 24 hours, cells were labelled and imaged.

Immunoblotting and Immunoprecipitation

Both phosphorylation and ubiquitination of TrkA constructs were monitored after TrkA immunoprecipitation. 24 to 48 h after transfection, SHSY5Y cells and HEK293T/17 were starved for two hours in DMEM/F-12 medium devoid serum. Then they were incubated for 10 minutes at 37°C in starvation medium, either in absence or presence of 125 ng/ml mouse NGF (NGF, Alomone Labs), and finally lysed. The following are the primary antibodies used: anti-TrkA (06-574, dilution 1:1000), anti-phosphotyrosine (05-321, dilution 1:1000) were from Millipore; anti-Trk C-14 (sc-11, pan-Trk) and anti-P4D1 (sc-8017, multimonoubiquitin and polyubiquitin antibody) were from Santa Cruz Biotechnology. Briefly, transfected cells were lysed in RIPA buffer (Sigma Aldrich) supplemented with phosphatase and protease inhibitor tablets (PhosSTOP™cOmplete™, EDTA-free Protease Inhibitor Cocktail, Sigma Aldrich). Total cell extracts (500 µg) were incubated with the pan-Trk antibody overnight at 4°C under rotary shaking. The mixture of antibody and lysates were then incubated 30 minutes at room temperature with Dynabeads protein A (Termo Fisher Scientific), previously washed three times with phosphate buffer saline with 0.002% Tween-20 (PBST). Alternatively, TrkA constructs were biotinylated as described [2], and the obtained lysates incubated with Dynabeads MyOneC1 (Termo Fisher Scientific) for 40 min at room temperature. The resulting complexes in the mixture were then magnetically isolated and beads washed three times with PBST, and then boiled in 2X Laemmli loading buffer at 95 °C for 10 minutes. Samples were then loaded on a gel (4-12 % pre-cast gradient gel, or a 4-20 % Criterion TGX Stain-free pre-cast gel, Biorad) and electrotransferred on a PVDF membrane (Immobilon®-P PVDF Membrane, Millipore, or Trans-Blot Turbo, Biorad). Criterion TGX Stain-Free gels were activated for 1 min after SDS–electrophoresis and imaged, before and after transfer, using the ChemiDoc MP imaging system (Bio-Rad).

Membranes were blocked for 1 hour at RT with Tris Buffered Saline+ 0.05% Tween-20 (TBST) supplemented with 5% w/v not-fat dry milk (Biorad) for the ubiquitination assay, and with TBST+ 5% w/v BSA (Sigma) for the phosphorylation assay. After blocking, membranes were blotted for 2.5 hours at RT or overnight at 4°C with anti-P4D1 and anti-phosphotyrosine. The primary antibodies were detected by using an anti-mouse or rabbit secondary antibody horseradish peroxidase (HRP)-conjugated (diluted 1:2500). Serum starved sub-confluent GM7373 cells were stimulated with 30 ng/mL of VEGF-A for 5 minutes. Cells were then lysed in lysis buffer [50 mmol/L Tris-HCl buffer (pH 7.4) containing 150 mmol/L NaCl, 1% Triton X-100, 1 mmol/L Na_3VO_4, and protease and phosphatase inhibitors (Sigma)]. Next, 50 µg of total cell lysate were separated by SDS–PAGE and probed with anti-phospho-VEGFR2 antibody (pTyr1175, Cell Signaling Technology, Beverly, MA), or with anti-VEGFR2 antibody (Santa Cruz Biotechnology) in a Western blot. Blotted membranes were incubated with Clarity Western ECL substrate or Clarity Max Western ECL substrate (Biorad) and signal detected with Image Quant LAS 4000 mini (Amersham) or ChemiDoc MP imaging system (Bio-Rad). Densitometric analysis of the obtained bands was done with ImageJ software (https://imagej.nih.gov/ij/) or ImageLab software (Bio-Rad). Analysis included the determination of total Stain-Free signal intensities of each sample lane on the blots. TrkA signals were automatically normalized using ImageLab software with Stain-Free total lane volumes.

FluoNGF binding assay

SHSY5Y cells were transfected with TrkA constructs. After 5 hours from transfection, they were trypsinized and seeded on glass slides at medium-high density. Next day, cells were serum starved for 2 hours. Surface receptors were then exposed for 30 minutes at 37°C to 100 ng/ml purified Alexa647-NGF conjugate (fluoNGF, prepared as in [3]). After five washes in PBS, cells were fixed for 30 minutes at room temperature in 4% PFA, 4% sucrose in PBS, washed three times with PBS and one time with deionized water. Glass slides were then mounted with Fluoroshield™ and imaged at the TIRF microscope set in epifluorescence mode. Quantification of the NGF signal was performed by calculating the mean intensity of Alexa647 channel for GFP-positive cells (i.e. TrkA expressing cells).

SPT data analysis

Membrane dynamics of TrkA and VEGFR2 single particles was analyzed as previously described [4], [5]. Briefly, Imaris software 7.6.5 (Bitplane Scientific Software) was used to detect and localize single Qdot labelled-TrkA spots and to generate the relative trajectories. Spots of Qdots adhered to the glass outside the cell were discarded by considering the superposition of the TIRF and DIC images. The obtained trajectories were finally exported in MATLAB-compatible files exploiting the Imaris XT module. Trajectories were analyzed with the custom MatLab algorithms described previously [4], with minor modifications. Briefly, complex trajectories switching between diffusive and confined regimes were segmented into the relative subtrajectories and separated into simple, self-similar trajectories. The pool of all (sub)trajectories (called simply “trajectories” in text and captions) was classified as mobile or non-mobile as in [4], and analyzed to compute the following parameters: i) the short-lag-time average diffusion coefficient D and its uncertainty, calculated from the first two points of the mean square displacement (MSD) curve; ii) the confinement length L, i.e. the typical linear dimension of the area explored by non-mobile trajectories; iii) the γ coefficient and its uncertainty, calculated from the moment scaling spectrum (MSS) curve: γ is related to half the “anomalous diffusion parameter” [$\gamma <, \sim, > 0.5$ for subdiffusive, Brownian, and superdiffusive trajectories, respectively, [6]]. We plotted the experimental distributions of L for non-mobile trajectories, of D for mobile ones, and of γ versus D for all trajectories (considering always the number of spots in each trajectory, and also the parameter uncertainties in the last two cases; see also 2.13). Especially the last

kind of plot revealed the existence of several different motion types for both TrkA and VEGFR2, as also previously discussed [4]. Here, for the sake of simplicity, we identified three distinct motion macro-categories: diffusive, confined and immobile, on the basis of their D vs γ distributions as in Fig. S9. Accordingly, the fraction of TrkA and VEGFR2 receptors in these three categories was calculated and used to generate the stack-column histogram plots.

Supplementary tables

Table S1. Different kinase-null mutants of TrkA receptor reported in the literature. Numeration of amino acids corresponds to isoform II of human and rat cDNA sequences deposited in UniProtKB database (https://www.uniprot.org/uniprot/P04629).
Human K544 corresponds to rat K547.

TrkA cDNA sequence	Mutation	References
human	K544A	[7]
	K544R	[8]
	K544N	[9]
rat	K547A	[10] [11] [12]
	K547N	[13]
	K547N	[14]
	K547R	[15]
	D671A	[16]

Table S2. Different kinase-null mutants of VEGFR2 receptor reported in the literature. Numeration of amino acids corresponds to isoform I of the human and mouse cDNA sequences deposited in UniProtKB database (https://www.uniprot.org/uniprot/P35968; https://www.uniprot.org/uniprot/P35918).
Human K868 corresponds to mouse K866.

VEGFR2 cDNA sequence	Mutation	References
human	K868M	[17]
	K868R	[18]
	Y1054F/Y1059F	[19]
mouse (Chimeric Kinase Receptor)	K866R	[20]

Table S3. List of primers used in the mutagenesis procedure.

Construct	Mutation	Primers	
		Type	Sequence (5'->3')
***r*TrkA-K547N**	K547N	FW	GCTGGTGGCTGTCAACGCACTGAAGGAGACATC
		RV	GATGTCTCCTTCAGTGCGTTGACAGCCACCAGC
***r*TrkA-RM**	Y499F	FW	GGAGAACCCACAGTTCTTCAGTGATACCTGTGTC
		RV	GACACAGGTATCACTGAAGAACTGTGGGTTCTCC

	Y760F	FW	CTGCCCTCCTGATGTCTTCGCCATCATGGCGCGGC
		RV	GCCGCGCATGATGGCGAAGACATCAGGAGGGCAG
	Y794F	FW	CAGGCGCCACCGAGTTTCCTGGACGTTCTGGGC
		RV	GCCCAGAACGTCCAGGAAACTCGGTGGCGCCTG
***r*TrkA-KM**	Y679F	FW	CATGAGCAGGGACATCTTCAGCACAGACTACTACC
		RV	GGTAGTAGTCTGTGCTGAAGATGTCCCTGCTCATG
	Y683F	FW	CATCTACAGCACAGACTTCTACCGTGTGGGAGGTC
		RV	GACCTCCCACACGGTAGAAGTCTGTGCTGTAGATG
	Y684F	FW	CTACAGCACAGACTACTTCCGTGTGGGAGGTCGG
		RV	CCGACCTCCCACACGGAAGTAGTCTGTGCTGTAG
***r*TrkA-P791S**	P791S	FW	CCTTGGCACAGGCGTCACCGAGTTACCTGG
		RV	CCAGGTAACTCGGTGACGCCTGTGCCAAGG
***r*TrkA-K547R**	K547R	FW	ATGCTGGTGGCTGTCAGGGCACTGAAGGAGAC
		RV	GTCTCCTTCAGTGCCCTGACAGCCACCAGCAT
***h*TrkA-K544N**	K544N	FW	GCTGGTGGCTGTCAGGGCACTGAAGGAGGCG
		RV	CGCCTCCTTCAGTGCGTTGACAGCCACCAGC
***m*VEGFR2-K866N**	K866N	FW	ACTTGCAAAACAGTAGCCGTCAACATGTTGAAAGAAGGAGCA
		RV	TGCTCCTTCTTTCAACATGTTGACGGCTACTGTTTTGCAAGT
***m*VEGFR2-K866R**	K866R	FW	ACTTGCAAAACAGTAGCCGTCCGGATGTTGAAAGAAGGAGCA
		RV	TGCTCCTTCTTTCAACATCCGGACGGCTACTGTTTTGCAAAGT

Table S4. Tabulated fractions of diffusive, confined and immobile receptors, referred to the stack-column histograms of Fig.1, Fig.2, Fig.4 and Fig.5.

TrKA-construct	Diffusive	Confined	Immobile
TrkA-wt (Fig.1, Fig.2)	0.62	0.32	0.06
TrkA-K547N (Fig. 1, Fig.2)	0.37	0.54	0.09
TrkA-RM(Fig.2)	0.59	0.37	0.04
TrkA-KM (Fig.2)	0.60	0.32	0.06
TrkA-K547R (Fig.2)	0.62	0.32	0.08
TrkA-P791S (Fig.2)	0.57	0.34	0.08

TrkA-wt UN (Fig.4)	0.62	0.32	0.06
TrkA-wt CD (Fig.4)	0.48	0.29	0.22
TrkA-wt LB (Fig.4)	0.22	0.37	0.40
TrkA-wt JK (Fig.4)	0.40	0.55	0.05
TrkA-K547N UN (Fig.4)	0.37	0.54	0.09
TrkA-K547N CD (Fig.4)	0.61	0.32	0.06
TrkA-K547N LB (Fig.4)	0.61	0.38	0.005
TrkA-K547N JK (Fig.4)	0.26	0.62	0.12
TrkA-wt +NGF (Fig. 1 and 5)	0.19	0.41	0.40
TrkA-K547N +NGF (Fig.1 and 5)	0.20	0.61	0.18
TrkA-RM +NGF (Fig.5)	0.49	0.30	0.20
TrkA-KM +NGF (Fig.5)	0.49	0.34	0.17
TrkA-K547R+NGF (Fig.5)	0.43	0.44	0.13
TrkA-P791S +NGF (Fig.5)	0.50	0.42	0.08

Supplementary Figure and Video Legends

Videos S1 and S2 (related to Fig.1C): Videos of S-Qdot-conjugated TrkA-wt (S1) and TrkA-K547N (S2) receptors in a living SHSY5Y cell previously transfected and labelled as described in the Methods section. Total video time: 10.5 seconds each.

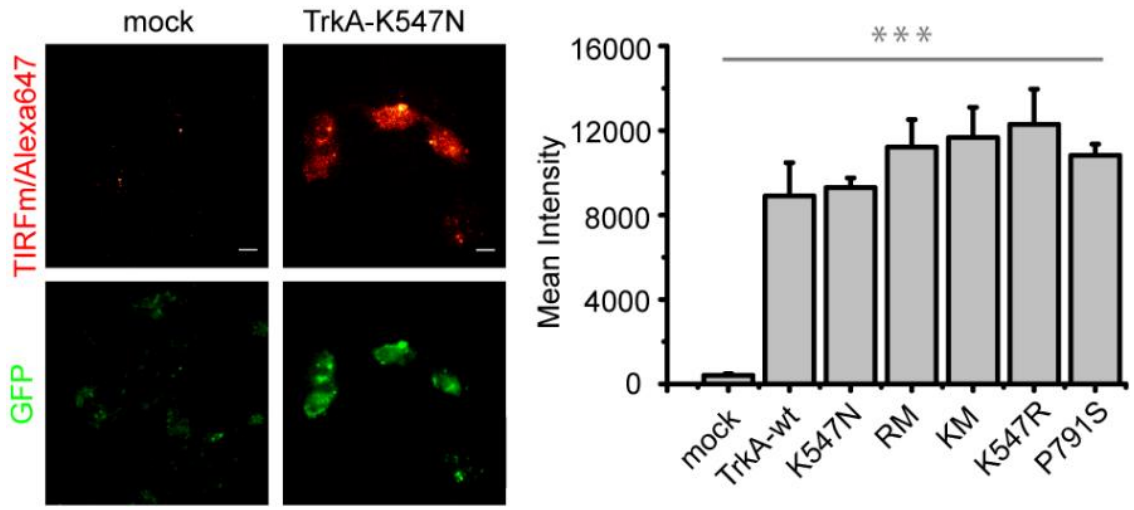

Fig.S1. Left: Representative TIRF images of SHSY5Y cells not-transfected (mock, left) and expressing *r*TrkA-K547N along with GFP (right), after incubation with Alexa647-labelled NGF; scale bar: 10 µm. Right: the corresponding quantification of Alexa647 mean intensity±sem, imaged at the surface of plasma membrane of SHSY5Y expressing *r*TrkA-wt or its mutants, compared to the same signal in non-transfected cells. We measured up to 20 cells pooled from two independent cover slips. ***p<0.001 according to one-way ANOVA with Bonferroni's Multiple Comparison test.

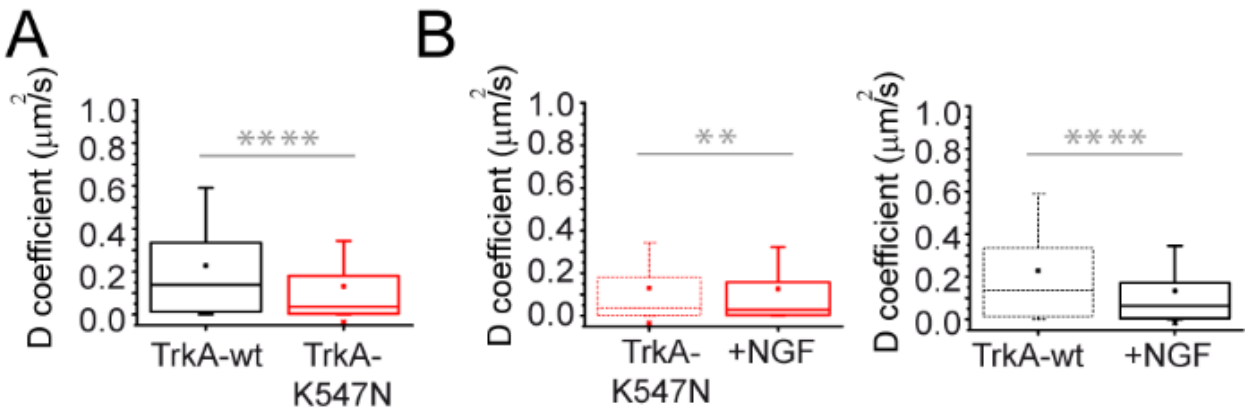

Fig. S2. Box-plot for D values retrieved from trajectories (at least 6 frames long) of: **A)** *r*TrkA-wt (red, n=1116) versus *r*TrkA-K547N (black, n=2640) in SHSY5Y cells in resting conditions, **B)** Left: *r*TrkA-K547N before (red dotted line, n=1116) and after NGF stimulation (red solid line, n=2909). Right: *r*TrkA-wt before (black dotted line, n=) and after NGF stimulation (black solid line,n=529). Trajectories are pooled from three independent measures. Boxes: 25th-75th percentiles; whiskers: 10th-90th percentile; line: median; square: mean. ****P<0.0001, **P<0.01, according to Mann-Whitney test.

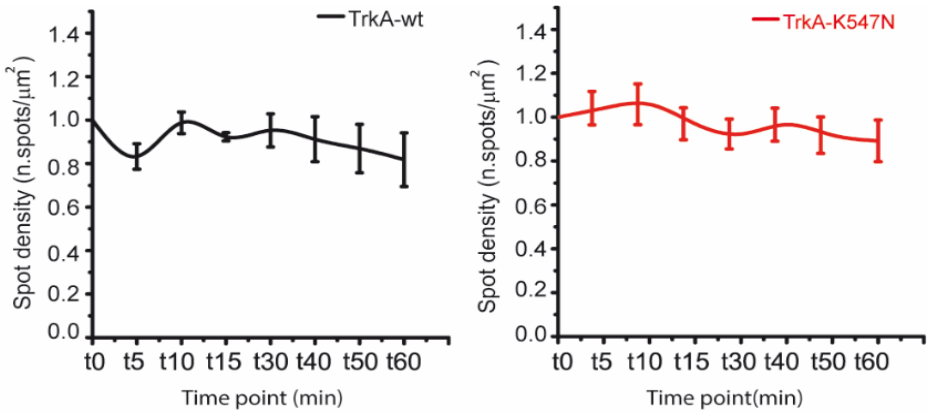

Fig. S3. Surface density quantification for *r*TrkA-wt and *r*TrkA-K547N spots at the different time points in the absence of NGF stimulation. Each value is plotted as mean±sem of the data from the same cells (n=5) acquired at different times, normalized by the spot density measured at time 0 for the corresponding cell. Differences at different times point for each construct are not significant according to one-way ANOVA with Bonferroni's Multiple Comparison test.

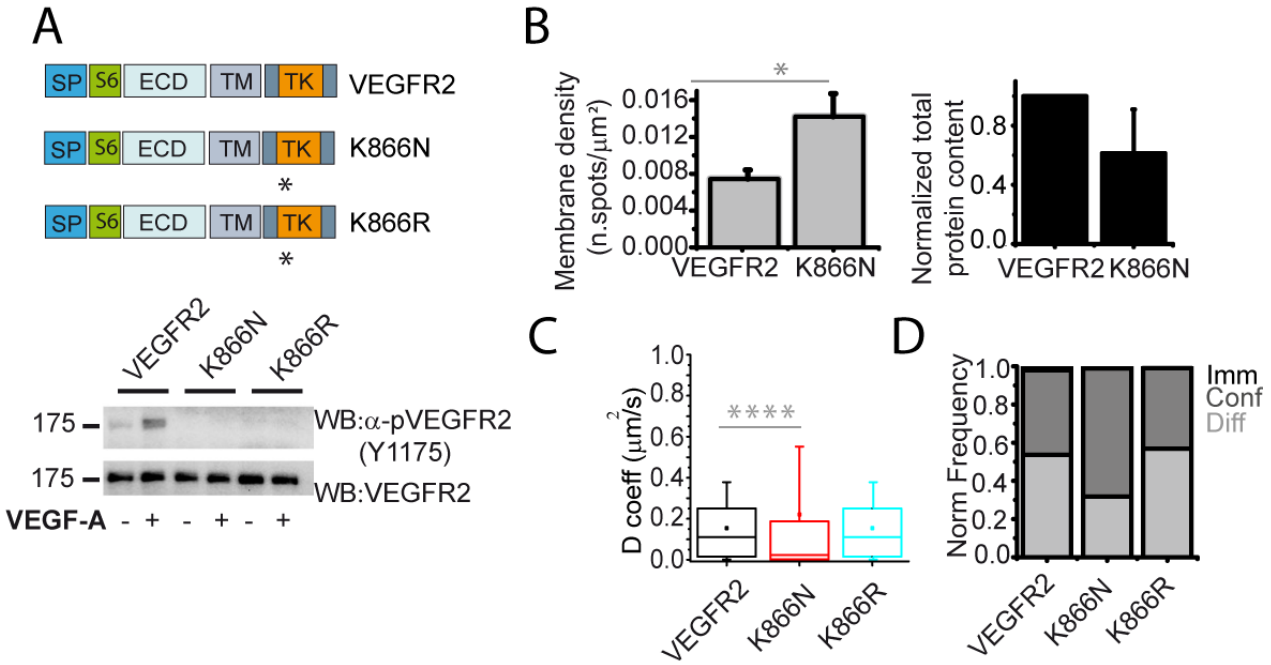

Fig.S4. A) Scheme of *m*VEGFR2-wt, *m*VEGFR2-K866N and *m*VEGFR2-K866R constructs (SP: signal peptide, S6: labelling tag, ECD: extracellular domain, TM: transmembrane domain, TK: Tyrosine Kinase domain inside the intracellular one); the asterisk highlights where the single point mutation is located. Below: western blot from cell extracts of GM7373-WT and GM7373-K866N shows phosphorylated VEGFR2 (p-VEGFR2; pTyr 1175) in presence or absence of 5 minutes stimulation with 30 ng/ml of VEGF-A. Total VEGFR2 was blotted as control. The GM7373 cell line, derived from bovine immortalized endothelial cells, lost the endogenous receptor and is therefore optimal for evaluation of VEGFR2 constructs [21]. **B)** Left: Membrane receptor density, quantified as number of Qdot-labelled moving spots visualized at TIRF per cell membrane area, for *m*VEGFR2-wt (n=10 cells) and

*m*VEGFR2-K866N (n=12 cells) receptors. *P<0.05 according to two-tailed Mann-Whitney test. Right: densitometric analysis of total *m*VEGFR2-wt and *m*VEGFR2-K866N content obtained averaging two blots; the densitometric content of *m*VEGFR2-K866N was normalized to that of the *m*VEGFR2-wt. **C)** Box-plot for D values retrieved from trajectories (at least 6 frames long) of *m*VEGFR2-wt (red, n=291), *m*VEGFR2-K866N (red, n=384) or *m*VEGFR2-K866R (cyano, n=512) in SHSY5Y cells in resting conditions. Trajectories are pooled from three independent measures. Boxes: 25^{th}-75^{th} percentiles; whiskers: 10^{th}-90^{th} percentile; line: median; square: mean. ****P<0.0001, according to Kruskal-Wallis test with Dunn's means comparison**. D)** Fraction of receptors undergoing diffusive (light-grey), confined (grey), immobile (black) motion modes for *m*VEGFR2-wt (n=10 cells, 355 trajectories), *m*VEGFR2-K866N (n=12 cells, 597 trajectories) and *m*VEGFR2-K547R (n=10 cells, 512 trajectories) in GM7373 cells in resting conditions. The total number of receptor spots (corresponding to n≥900 trajectories) was normalized to 1.

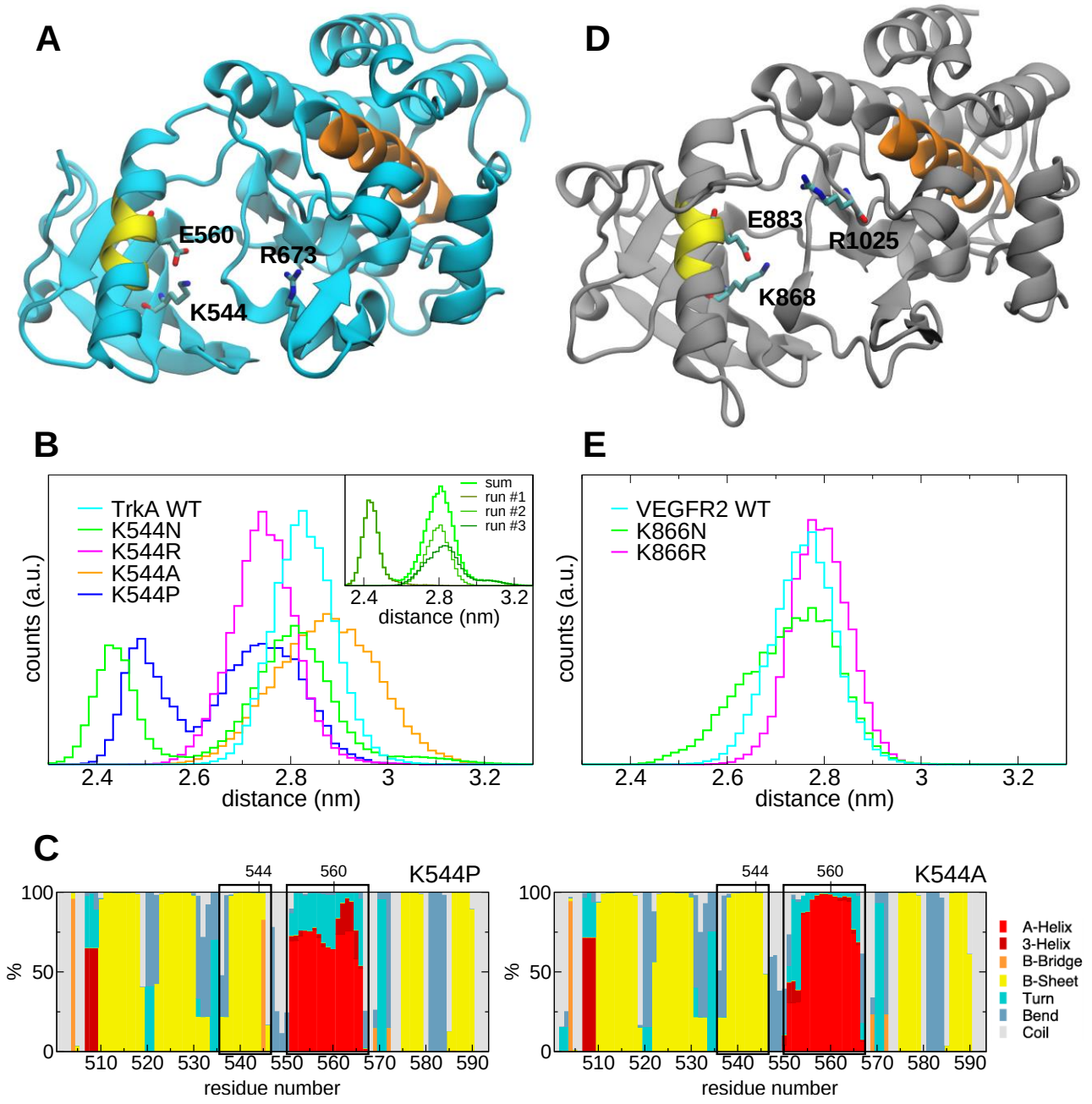

Fig. S5. A) Crystal structure of *h*TrkA (4f0i, in cyan) and **D)** *h*VEGFR2 (6gqq, in gray) highlighting in yellow the region of the αC helix containing Glu560 *h*TrkA (Glu883 in *h*VEGFR2) and in orange the αF helix. The image also shows the amino acids involved in the native salt-bridge (Lys544-Glu560 in *h*TrkA, and Lys866-Glu883 in *h*VEGFR2) and the Arg residue (Arg673 in *h*TrkA and Arg1025 in *h*VEGFR2) involved in the formation of the new salt-bridge during the MD simulations of the K544N and K868N. **B** and **E)** Histogram plots of the distance between the region of the αC helix containing Glu560/883 (a.a. 558-562 in *h*TrkA and a.a. 881-885 in *h*VEGFR2) and αF helix in the C-lobe (a.a. 707-722 in *h*TrkA and a.a. 1084-1099 in *h*VEGFR2) during the combined MD simulations for the wt proteins and the indicated mutants: *h*TrkA-wt (cyan), *h*TrkA-K544N (green), *h*TrkA-K544R (magenta), *h*TrkA-K544A (orange) and *h*TrkA-K544P (blue) in panel **B** and *h*VEGFR2-wt (cyan), *h*VEGFR2-K544N (green), *h*VEGFR2-K544R (magenta) in panel **E**. The distance is calculated between the centers of mass of the α-carbons in each region. The inset in panel **B** shows the separate histograms for each of the three MD simulations of *h*TrkA- K544N (see methods) in different shades of green, together with their sum. **C)** Secondary-structure

stacked histograms of the N-lobe in the *h*TrkA-K544A and *h*TrkA-K544P mutants, derived from the MD simulations, reported for a comparison with Fig. 2C.

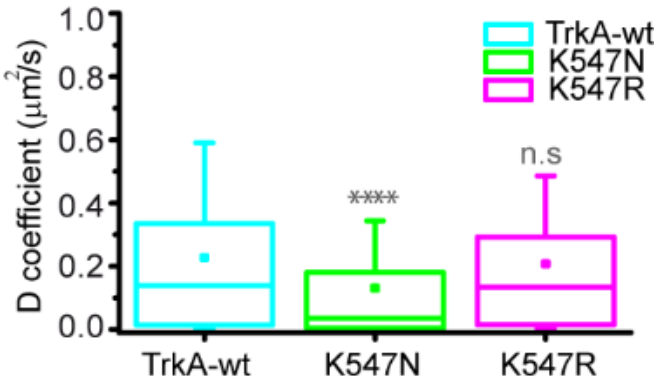

Fig.S6. Box-plot for D values retrieved from trajectories (at least 6 frames long) of *r*TrkA-wt (red, n=1116), *r*TrkA-K547N (green, n=2640) or *r*TrkA-K547R (blue, n=1313) in SHSY5Y cells in resting conditions. Trajectories are pooled from three independent measures. Boxes: 25th-75th percentiles; whiskers: 10th-90th percentile; line: median; square: mean. ****P<0.0001, n.s.: non-significant at the 0.05 level, according to Kruskal-Wallis test, with Dunn's means comparison.

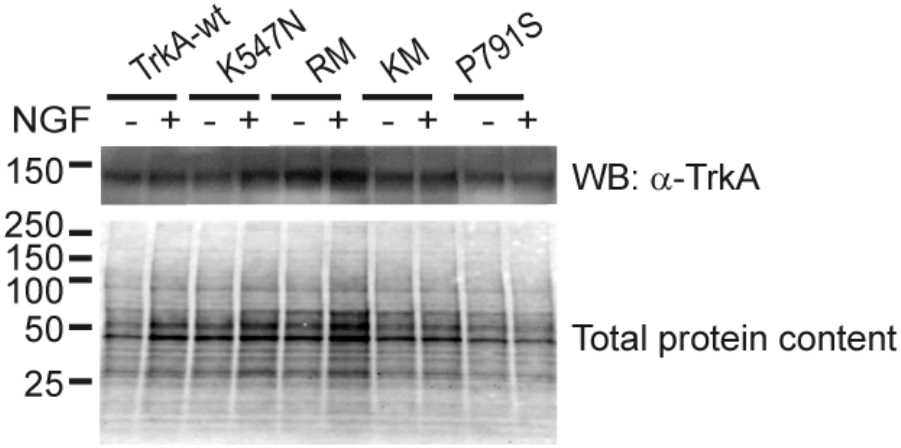

Fig.S7. Top: WB showing total TrkA levels for the same samples shown in Fig 5A. Bottom: total protein content for each lane of the blot visualized using the Stain-Free^{TM} technology by Biorad. The total protein content was used for normalization of TrkA signals.

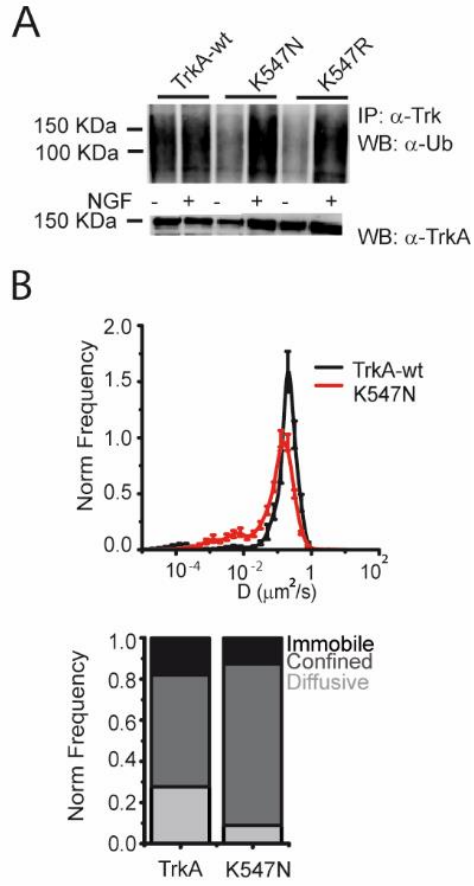

Fig.S8. A) WB showing total ubiquitination levels in the absence (-) or presence (+) of 10 minutes stimulation with 125 ng/ml NGF, in HEK293T cells transfected with *r*TrkA-wt, *r*TrkA-K547N and *r*TrkA-K547R constructs. Cell lysates were immunoprecipitated (IP) with anti-Trk (C-14) antibody, and subsequently blotted with P4D1 antibody recognizing both mono- and poly- ubiquitin, stripped and re-blotted with anti-TrkA antibody. **B)** Top: Distribution of diffusion coefficient (D) and estimated uncertainty obtained for mobile *r*TrkA-wt (black curve, n=11 cells, 924 trajectories) and *r*TrkA-K547N (red curve, n=15 cells, 2407 trajectories) trajectories in HEK293 cells. Bottom: stack-column histogram plot for the fraction of diffusive (light-grey), confined (grey), immobile (black) receptors obtained in the same experiments.

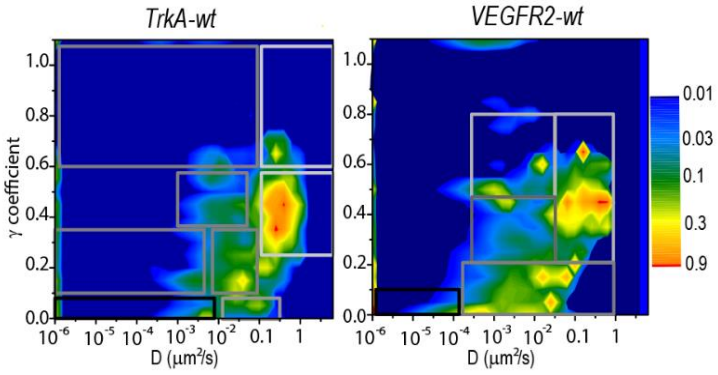

Fig.S9. Total D-γ distributions according to MSS-TAD analysis [4] for *r*TrkA-wt (n=13 cells, 1989 trajectories) and *m*VEGFR2-wt (n= 10 cells, 355 trajectories) in non-stimulated cells. The diffusion coefficient D reflects the short-term diffusivity and the γ factor reflects the long-term trajectory behavior. On the right, logarithmic-scale color code for the frequency of the total D-γ distributions, normalized to 1 at the peak. D-γ regions highlighted by the light-gray, gray and black boxes superimposed on each plot correspond to trajectories respectively classified as diffusive, confined and immobile in this paper.

Supplementary References

[1] J. B. Grinspan, S. N. Mueller, and E. M. Levine, "Bovine endothelial cells transformed in vitro by benzo(a)pyrene," *J. Cell. Physiol.*, 1983.

[2] F. Gobbo, F. Bonsignore, R. Amodeo, A. Cattaneo, and L. Marchetti, "Site-specific direct labeling of neurotrophins and their receptors: From biochemistry to advanced imaging applications," in *Methods in Molecular Biology*, vol. 1727, 2018, pp. 295–314.

[3] P. Di Matteo, M. Calvello, S. Luin, L. Marchetti, and A. Cattaneo, "An Optimized Procedure for the Site-Directed Labeling of NGF and proNGF for Imaging Purposes," *Front. Mol. Biosci.*, vol. 4, no. February, pp. 1–9, 2017.

[4] L. Marchetti *et al.*, "Ligand signature in the membrane dynamics of single TrkA receptor molecules," *J. Cell Sci.*, vol. 126, no. 19, pp. 4445–4456, 2013.

[5] A. Callegari, S. Luin, L. Marchetti, A. Duci, A. Cattaneo, and F. Beltram, "Single particle tracking of acyl carrier protein (ACP)-tagged TrkA receptors in PC12nnr5 cells," *J. Neurosci. Methods*, vol. 204, no. 1, pp. 82–86, 2012.

[6] R. B. Best and G. Hummer, "Optimized molecular dynamics force fields applied to the helix-coil transition of polypeptides," *J. Phys. Chem. B*, 2009.

[7] S. Jing, P. Tapley, and M. Barbacid, "Nerve growth factor mediates signal transduction through trk homodimer receptors," *Neuron*, vol. 9, no. 6, pp. 1067–1079, 1992.

[8] R. Singh *et al.*, "TRAF4-mediated ubiquitination of NGF receptor TrkA regulates prostate cancer metastasis," *J. Clin. Invest.*, vol. 128, no. 7, pp. 3129–3143, 2018.

[9] R. M. Stephens, D. M. Loeb, T. D. Copeland, T. Pawson, L. A. Greene, and D. R. Kaplan, "Trk receptors use redundant signal transduction pathways involving SHC and PLC-γ1 to mediate NGF responses," *Neuron*, vol. 12, no. 3, pp. 691–705, 1994.

[10] H. Yano, F. Cong, R. B. Birge, S. P. Goff, and M. V. Chao, "Association of the Abl tyrosine kinase with the Trk nerve growth factor receptor," *J. Neurosci. Res.*, 2000.

[11] H. Yano *et al.*, "Association of Trk neurotrophin receptors with components of the cytoplasmic dynein motor.," *J. Neurosci.*, 2001.

[12] L. Harel *et al.*, "CCM2 Mediates Death Signaling by the TrkA Receptor Tyrosine Kinase," *Neuron*, 2009.

[13] J. Jullien, V. Guili, E. A. Derrington, J. L. Darlix, L. F. Reichardt, and B. B. Rudkin, "Trafficking of TrkA-green fluorescent protein chimerae during nerve growth factor-induced differentiation," *J. Biol. Chem.*, vol. 278, no. 10, pp. 8706–8716, 2003.

[14] S. J. Dixon, J. I. S. MacDonald, K. N. Robinson, C. J. Kubu, and S. O. Meakin, "Trk receptor binding and neurotrophin/fibroblast growth factor (FGF)-dependent activation of the FGF receptor substrate (FRS)-3," *Biochim. Biophys. Acta - Mol. Cell Res.*, vol. 1763, no. 4, pp. 366–380, 2006.

[15] J. C. Arevalo *et al.*, "Cell survival through Trk neurotrophin receptors is differentially regulated by ubiquitination," *Neuron*, vol. 50, no. 4, pp. 549–559, 2006.

[16] L. C. Schecterson *et al.*, "Trk activation in the secretory pathway promotes Golgi

fragmentation," *Mol. Cell. Neurosci.*, vol. 43, no. 4, pp. 403–413, 2010.
[17] T. Takahashi, S. Yamaguchi, K. Chida, and M. Shibuya, "A single autophosphorylation site on KDR/Flk-1 is essential for VEGF-A-dependent activation of PLC-γ and DNA synthesis in vascular endothelial cells," *EMBO J.*, vol. 20, no. 11, pp. 2768–2778, 2001.
[18] M. G. Blanes, M. Oubaha, Y. Rautureau, and J. P. Gratton, "Phosphorylation of tyrosine 801 of vascular endothelial growth factor receptor-2 is necessary for Akt-dependent endothelial nitric-oxide synthase activation and nitric oxide release from endothelial cells," *J. Biol. Chem.*, vol. 282, no. 14, pp. 10660–10669, 2007.
[19] C. M. Warren, S. Ziyad, A. Briot, A. Der, and M. L. Iruela-Arispe, "A ligand-independent VEGFR2 signaling pathway limits angiogenic responses in diabetes," *Sci. Signal.*, vol. 7, no. 307, pp. 1–12, 2014.
[20] A. J. Singh, R. D. Meyer, H. Band, and N. Rahimi, "The carboxyl terminus of VEGFR-2 is required for PKC-mediated down-regulation," *Mol. Biol. Cell*, 2005.
[21] C. Ravelli, E. Grillo, M. Corsini, D. Coltrini, M. Presta, and S. Mitola, "β<inf>3</inf> Integrin promotes long-lasting activation and polarization of vascular endothelial growth factor receptor 2 by immobilized ligand," *Arterioscler. Thromb. Vasc. Biol.*, vol. 35, no. 10, pp. 2161–2171, 2015.